Journal of Marine Systems 78 (2009) 442–459

Contents lists available at ScienceDirect

Journal of Marine Systems

journal homepage: www.elsevier.com/locate/jmarsys

Asymmetry of Columbia River tidal plume fronts

David A. Jay [a,*], Jiayi Pan [a], Philip M. Orton [b], Alexander R. Horner-Devine [c]

[a] Department of Civil and Environmental Engineering, Portland State University, PO Box 751, Portland, OR 97201, USA
[b] Ocean and Climate Physics, Lamont Doherty Earth Observatory, Columbia University, 61 Route 9W, Palisades, NY 10964, USA
[c] Department of Civil and Environmental Engineering, University of Washington, Box 352700, Seattle, WA 98195-2700, USA

ARTICLE INFO

Article history:
Received 9 October 2006
Received in revised form 1 April 2008
Accepted 12 November 2008
Available online 14 February 2009

Keywords:
Plumes
Fronts
Internal waves
Tidal effects
California current
Upwelling

ABSTRACT

Columbia River tidal plume dynamics can be explained in terms of two asymmetries related to plume-front depth and internal wave generation. These asymmetries may be an important factor contributing to the observed greater primary productivity and phytoplankton standing crop on the Washington shelf. The tidal plume (the most recent ebb outflow from the estuary) is initially supercritical with respect to the frontal internal Froude number F_R on strong ebbs. It is separated from the rotating plume bulge by a front, whose properties are very different under upwelling vs. downwelling conditions. Under summer upwelling conditions, tidal plume fronts are sharp and narrow (<20–50 m wide) on their upwind or northern side and mark a transition from supercritical to subcritical flow for up to 12 h after high water. Such sharp fronts are a source of turbulent mixing, despite the strong stratification. Because the tidal plume may overlie newly upwelled waters, these fronts can mix nutrients into the plume. Symmetry would suggest that there should be a sharp front south of the estuary mouth under summer downwelling conditions. Instead, the downwelling tidal plume front is usually diffuse on its upstream side. Mixing is weaker, and the water masses immediately below are low in nutrients. There is also an upwelling–downwelling asymmetry in internal wave generation. During upwelling and weak wind conditions, plume fronts often generate trains of non-linear internal waves as they transition from a supercritical to a subcritical state. Under downwelling conditions, internal wave release is less common and the waves are less energetic. Furthermore, regardless of wind conditions, solition formation almost always begins on the south side of the plume so that the front "unzips" from south to north. This distinction is important, because these internal waves contribute to vertical mixing in the plume bulge and transport low-salinity water across the tidal plume into the plume bulge.

F_R and plume depth are key parameters in distinguishing the upwelling and downwelling situations, and these two asymmetries can be explained in terms of potential vorticity conservation. The divergence of the tidal outflow after it leaves the estuary embeds relative vorticity in the emerging tidal plume water mass. This vorticity controls the transition of the tidal plume front to a subcritical state and consequently the timing and location of internal wave generation by plume fronts.

1. Introduction

A buoyant river plume and its fronts interact strongly with ambient alongshore flow, influencing thereby vertical mixing, the nutrient supply to surface waters, and the transport of organisms and particles. These issues have been studied to date in several contexts (e.g., Chao, 1988; Fong et al., 1997; O'Donnell et al., 1998; Garcia-Berdeal et al., 2002; Hickey et al., 2005). Here, we consider the interaction of the Columbia River plume with the California Current. This interaction is important because it supports high levels of primary production and major fisheries in the Pacific Northwest (Landry et al., 1989), and because freshwater inflow is vital to the supply of micronutrients to the entire California Current upwelling regime (Lohan and Bruland, 2006).

More specifically, this paper investigates the interaction of the Columbia River tidal plume fronts with the California Current upwelling/downwelling regime. For this purpose, we use synthetic aperture radar (SAR) and ocean color data, vessel data collected 2004–2006 by the RISE (*R*iver-*I*nfluences on *S*helf *E*cosystems) project, and a scaling analysis. The "tidal plume" is the water from the most recent ebb. This usage reflects the fact that outflow from the Columbia River is discontinuous, occurring as distinct, high-velocity ebb pulses. The interactions of tidal plume fronts with the upwelling regime are of particular interest, because up to 20% of total mixing between river and ocean water occurs within 100 m behind the tidal plume front, even though this is <2% of total plume area (Orton and Jay, 2005). Internal waves spawned at the front cause additional mixing (Nash and Moum, 2005) not considered in the Orton and Jay estimate.

* Corresponding author. Tel.: +1 503 725 4247.
E-mail addresses: djay@cecs.pdx.edu (D.A. Jay), panj@cecs.pdx.edu (J. Pan), orton@ldeo.columbia.edu (P.M. Orton), arhd@u.washington.edu (A.R. Horner-Devine).

0924-7963/$ – see front matter © 2009 Elsevier B.V. All rights reserved.
doi:10.1016/j.jmarsys.2008.11.015

Discussion of the interaction of the tidal plume with the upwelling regime is conveniently framed in terms of the two asymmetries between tidal plume fronts observed during upwelling vs. downwelling periods. During summer upwelling periods, our observations show that the tidal plume fronts remain super-critical for many hours after they leave the estuary entrance, particularly on their upwind, northern side. They are sharp and narrow (20–50 m wide) and mark a transition from supercritical to sub-critical flow for up to 12 h after high water. Despite high stratification, these fronts and the internal waves they generate represent a source of vigorous turbulent mixing north of the estuary mouth. Symmetry would suggest that, under summer downwelling conditions, there should be a sharp front south (upwind) of the estuary mouth. In fact, tidal plume fronts under summer downwelling periods are usually broad and diffuse even on their upstream side, because a transition from supercritical to subcritical conditions has already occurred close to the estuary mouth. Less mixing is accomplished, and the water immediately below the plume consists of old plume and surface waters, both low in nutrients.

Internal wave generation by plume fronts is also asymmetric. Supercritical plume fronts often generate trains of non-linear internal waves (IW) as they transition to a subcritical state. SAR images presented herein show that internal wave formation occurs frequently under upwelling or neutral conditions, and less frequently under downwelling conditions. Moreover, IW formation begins on the south side of the tidal plume (regardless of wind forcing) and moves along the plume front so that the front "unzips" (undergoes fission) from south to north. This implies that a frontal transition from supercritical to subcritical conditions first occurs south of the estuary mouth, regardless of whether this is the upwind or downwind side of the plume. We show below that both of these asymmetries can be explained in terms of potential vorticity conservation.

2. Regional context

2.1. The plume and the California current

The Columbia is the fourth largest river entering the ocean from North America, with an average flow of ~7300 $m^3\ s^{-1}$. Flows vary between 2500 (fall) and 12,500 $m^3\ s^{-1}$ (spring) over a typical year, but reach 25,000 $m^3\ s^{-1}$ in major winter floods (Bottom et al., 2005). It is the largest single source of freshwater inflow along the Pacific Coast of the Americas. The Columbia plume is a dominant feature in the hydrography of the Oregon and Washington coasts, sometimes transporting particles, organisms, and contaminants hundreds of kilometers along and across the continental margin (Barnes et al., 1972; Thomas and Weatherbee, 2005, and Fig. 1). The highest regional rates of primary productivity and standing stock of chlorophyll are associated with regions influenced by freshwater in spring; i.e., the plume itself and the Washington shelf (Landry et al., 1989). These areas are also vital to the survival of juvenile salmonids, several races of which are classified as endangered. The spring and summer spatial extent of the plume has been greatly reduced by reduction of spring freshet volume by >40% due to flow regulation and irrigation diversion. Our analysis of fronts provides context for understanding the potential impacts of flow reduction.

Broadly speaking, the Columbia plume flows northward over the shelf during winter downwelling periods, and southward offshore of the shelf during summer upwelling (Figs. 2 and 3), but these canonical configurations can occur any time of year, because the plume changes direction, thickness and width in response to frequent local wind stress fluctuations (Hickey et al., 1998; Garcia-Berdeal et al., 2002). Weak winds or winds from the east can result in movement of the plume directly offshore, because of its high initial momentum. Periods of variable winds, especially frequent in May and June, result in a "bi-

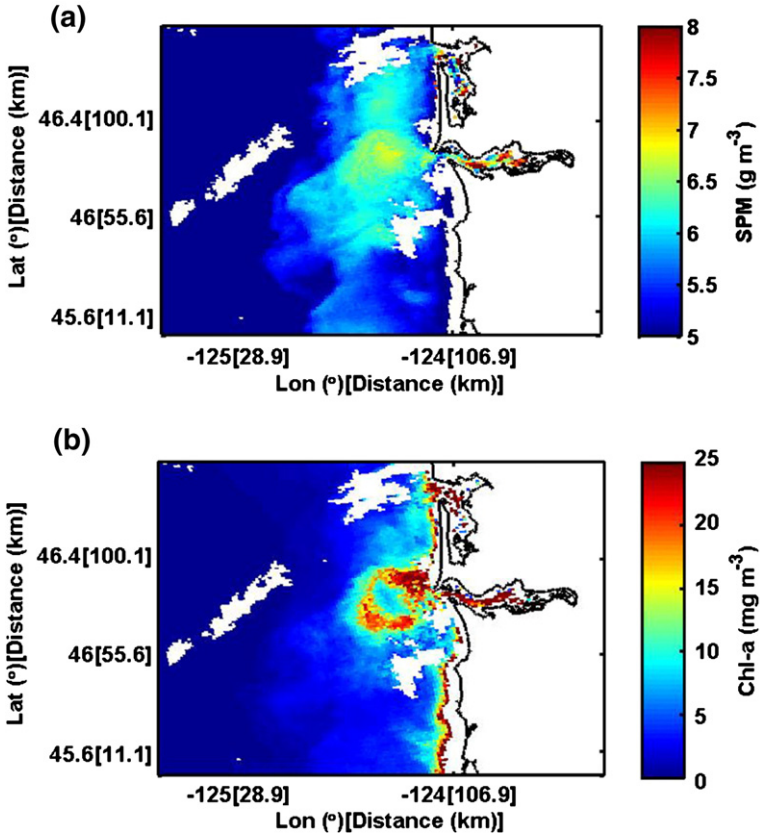

Fig. 1. The Columbia River plume and its influence shown in (a) by SPM and (b) by Chl-a; MODIS derived images for 12 July 2004 at 2130, 5 h after high water (lesser ebb, two days after a neap). Weak upwelling-favorable winds prevailed. River flow during the week prior to these images averaged ~5000 $m^3\ s^{-1}$, well below average for July. In (b), the circular plume bulge area of high productivity near the river mouth probably contains the water from several ebbs. High Chl-a levels are also seen along the coast, north and south of the river mouth. The bulk plume, as indicated by the SPM distribution trends southward and offshore; this is most evident in the SPM distribution. Old plume water is seen north of the river mouth.

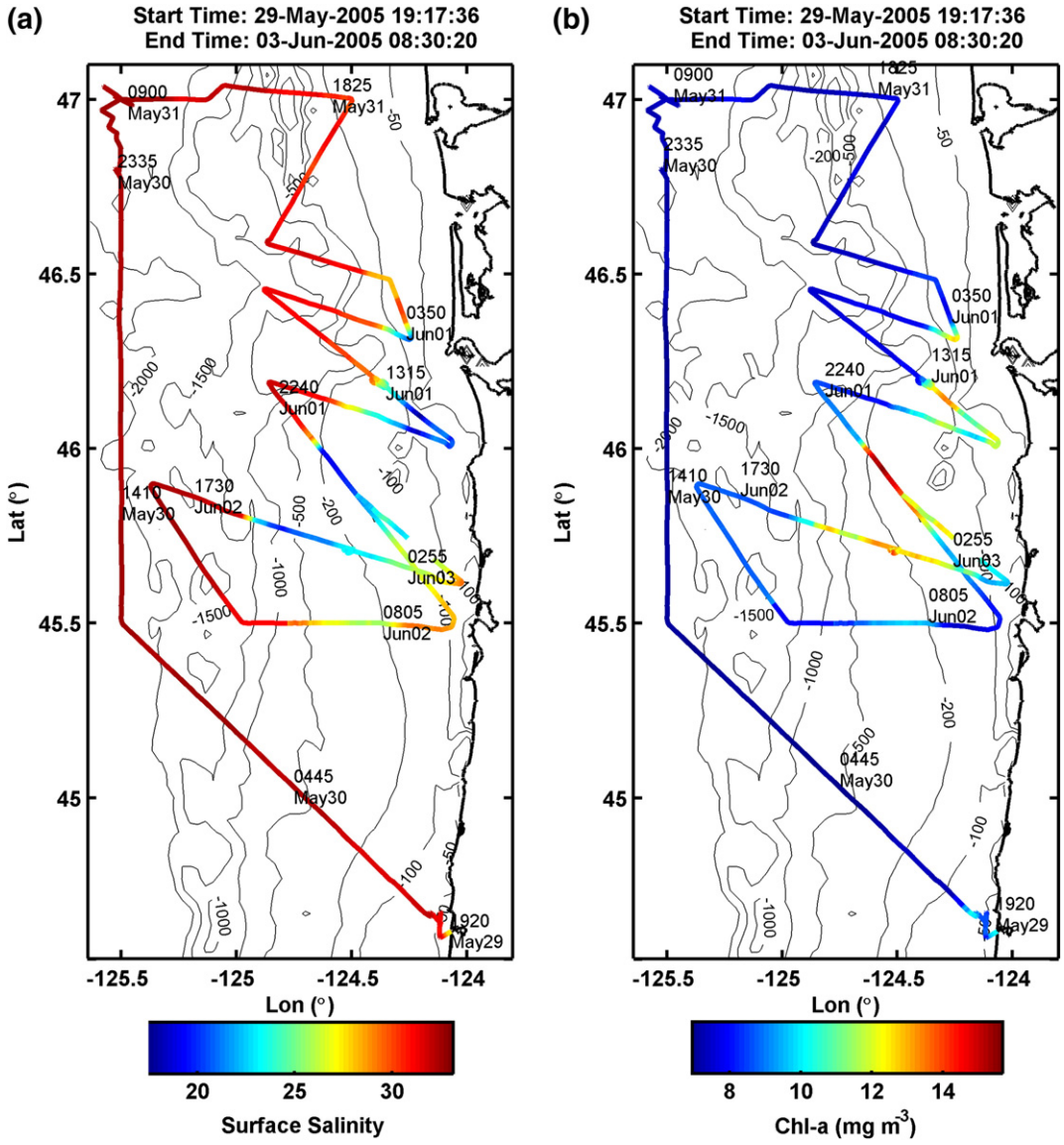

Fig. 2. Transition to upwelling: maps obtained 29 May to 3 June 2005 of salinity (a) and Chl-a (b) ~3 m below free surface during RISE-2; data are from the *R/V Pt. Sur* UDAS. Plume waters have moved southwestward under the influence of weak upwelling-favorable winds, but old plume waters remain at the surface along the coast except at the very south end of the map. The large volume of freshwater input by the spring freshet caps upwelled waters along the coast; elevated Chl-a levels are seen only within the plume. Several storms during May caused nutrient levels in river water to be above average for the season.

directional" plume with freshwater north and south of the river mouth (Hickey et al., 2005). Because of the very high buoyancy input, the plume near-field and bulge are very stratified, with the 3–10 m thick plume overlying shelf waters. In the parlance of Yankovsky and Chapman (1997), the Columbia plume is in the "surface-advected" category, due to the relatively narrow, steep shelf off the river mouth. It differs, therefore, from the more-studied Rhine plume, which usually has a lower buoyancy input and stronger tides, allowing mixing to sometimes extend to the bed (e.g., Souza and Simpson, 1997). The Columbia plume affects the bed only immediately beneath plume fronts and in the plume near-field (Orton and Jay, 2005; Spahn et al., submitted for publication).

RISE observations show that there are several reasons why the Columbia plume is itself highly productive and contributes to regional primary production:

- The paradoxical nature of plume mixing: Despite high stratification, plume fronts exhibit vigorous mixing and disturb the seabed down to at least 50–60 m (Orton and Jay, 2005). This contributes to mixing upwelled nutrients and iron (Fe) from re-suspended river sediments into the surface layer.
- Plume nutrients and micronutrients: The plume supplies nitrogen (N), phosphate (P), iron (Fe) and manganese (Mn) from land (Jay et al., 2002; Lohan and Bruland, 2006).
- Compensating production: Elevated riverine nutrient input to the plume due to precipitation over the coastal subbasin of the Columbia River partially compensates for primary production lost during periods of prolonged downwelling. This mechanism is most important during years like 2005 when strong upwelling is delayed until midsummer (cf. Fig. 2).

An important feature of the Pacific Northwest coastal ecosystem is that the standing stocks of chlorophyll and primary productivity are both higher on the Washington shelf than the Oregon shelf (Landry et al., 1989; Hickey, 1989). The fact that the movement of new plume water is often northward and onshore in a coastal current during downwelling vs. off-shelf and southward during upwelling is one factor that may explain this observation. The northward movement of Fe-rich silt during winter storms is another important factor. We suggest in Section 5 that differences between upwelling and downwelling tidal plume fronts are also important. Upwelling fronts exhibit

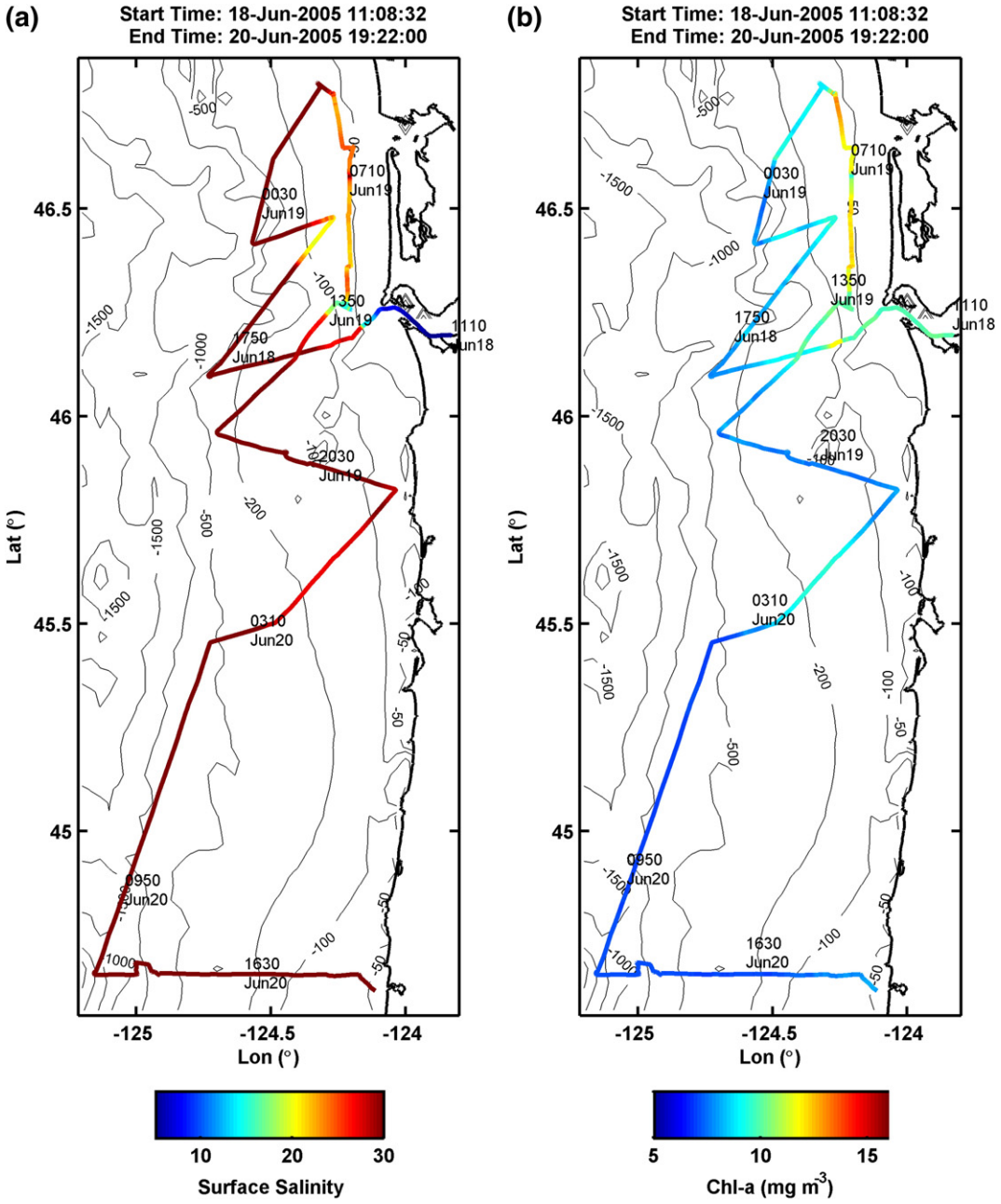

Fig. 3. Moderate downwelling winds: a map obtained 18–20 June 2005 of salinity (a) and Chl-a (b) ~3 m below free surface during RISE-2; data are from the *R/V Pt. Sur* UDAS. Low salinity, new plume water is found only in the near-field and north of the river mouth, though old plume water is found to the south. Downwelling-favorable winds reached 10 m s^{-1} on 17 June, but winds dropped to light and variable by the end of the survey period.

stronger mixing, and are more likely to mix plume and recently upwelled waters; this mixing occurs primarily north of the estuary mouth. Thus, frontal propagation provides a mechanism for mixing on the shelf and slope in the sense of Kelvin wave propagation (northward) relative to the estuary mouth, where it would otherwise be suppressed by the stratification of the plume.

2.2. Plume anatomy and function

Understanding plume processes requires terminology for plume functional components. Garvine (1982) divided a steady buoyant plume into three zones or regimes: a source zone, the near-field and the far-field. The Columbia plume, where a very strong tidal outflow overrides and interacts with a larger anticyclonic plume bulge, requires a distinction between the tidal plume and the remainder of the plume near-field. Thus, the Columbia plume has the following components (Fig. 3 in Horner-Devine et al., 2009-this volume):

- The plume source zone: The plume source zone is the area at the entrance of the estuary where low-salinity estuarine water lifts off from the seabed to form the nascent plume. Plume lift-off occurs at an internal hydraulic control (a width constriction associated with lateral stone jetty), near the landward boundary of the source zone (Cudaback and Jay, 1996, 2000). After lift-off, the plume flow is laterally confined by stone jetties for about 3 km before its expansion into the coastal ocean as a tidal plume. An internal hydraulic control is a common feature of plume lift-off in river estuaries (e.g., in the Fraser River, Macdonald and Geyer, 2004).
- The tidal plume: The tidal plume consists of the most recent ebb outflow from the plume and is surrounded by strong fronts (Orton and Jay, 2005; Nash and Moum, 2005). It remains distinct from the plume

bulge until its fronts become subcritical, after which time it gradually merges into the rotating plume bulge. Under weak wind forcing conditions, the plume is semicircular to circular. Typical tidal plume diameters are 10–35 km. The scaling of the tidal-plume and plume bulge is considered in Horner-Devine et al. (2009-this volume).

- The plume bulge: The bulge surrounds the tidal plume under most wind conditions (but may be displaced and diminished in size during periods of strong winds from the south). It usually contains the water from several ebbs and is separated from the plume far-field by a diffuse frontal zone.
- The plume far-field: The far-field is the zone beyond the bulge where final mixing of plume and ambient seawater occurs; $S = 32$ to 32.5 defines its outer boundary (Barnes et al., 1972).

In addition to these four components, we also refer to the plume as a whole as the "bulk plume."

These four zones provide a good basis for a detailed description of the features of Columbia tidal plume fronts and the internal waves generated at these fronts. It is also useful to define a "front." A front is a distinct boundary between two water masses. Tidal plume fronts occur through convergence in the presence of a buoyancy gradient imposed by river inflow. A convergent front, especially one that is super-critical, will have a well defined "head" or plunge at the visible surface signature, followed by a broader area of elevated mixing (O'Donnell et al., 2008).

3. Methods: data collection and processing

Sampling the Columbia River plume is challenging, because it is shallow (2–10 m) and highly mobile. It also varies on time scales of less than a day and is characterized by length scales that are difficult to cover synoptically with a single vessel (Hickey et al., 1998). Therefore, remote sensing data and results from towed vehicle (TRIAXUS) sampling are used herein. Despite the ~3 m s^{-1} tow speed of TRIAXUS, it was necessary to alternate between two sampling modes: a) plume scale maps of 2–3 d duration, and b) process studies in a limited area, with 2–6 h repeat times.

RISE physical oceanography was carried out on *R/V Pt Sur*. The *R/V Pt Sur* performed rapid surveys using a towed body (the TRIAXUS, steerable in 3D) and the vessel's near-surface underway data acquisition system or UDAS (nominally at 3 m depth). The high mobility of TRIAXUS was used to sample surface waters (up to within 0.5–2 m of the surface, depending on sea state) outside of the ship wake. TRIAXUS was used during three cruises. RISE1 (July 2004) occurred during a period of decreasing river flow after a weak spring freshet; prolonged upwelling was seen at the end of the cruise. RISE2 (June 2005) occurred during decreasing river flow after a weak spring freshet; strong upwelling was absent. RISE4 (June 2006) had moderately high but decreasing river flow; some weak upwelling was observed.

Instrumentation was as follows. The *R/V Pt Sur* carried a pole-mounted acoustic Doppler current profiler (ADCP; 300 kHz for RISE1, 1200 kHz for RISE2 and RISE4). The UDAS acquired position, meteorological data, salinity (S), temperature (T), and fluorescence at 3 m. TRIAXUS carried a 911 SeaBird conductivity–temperature–depth (CTD) profiler equipped with sensors for nitrate (N), C, T, pressure, transmissivity and fluorescence, and other instruments not relevant here. CTD casts were made at the beginning and end of maps with a second, identical SeaBird 911 CTD for calibration purposes. The vessel and pole-mounted ADCP data sets and TRIAXUS scalar data are used in the analyses described herein.

Synthetic aperture radar (SAR) and ocean color images are used in this study to provide synoptic coverage of the plume area. SAR images were obtained from RADARSAT-1. The SAR data were archived and distributed through the Comprehensive Large Array-data Stewardship

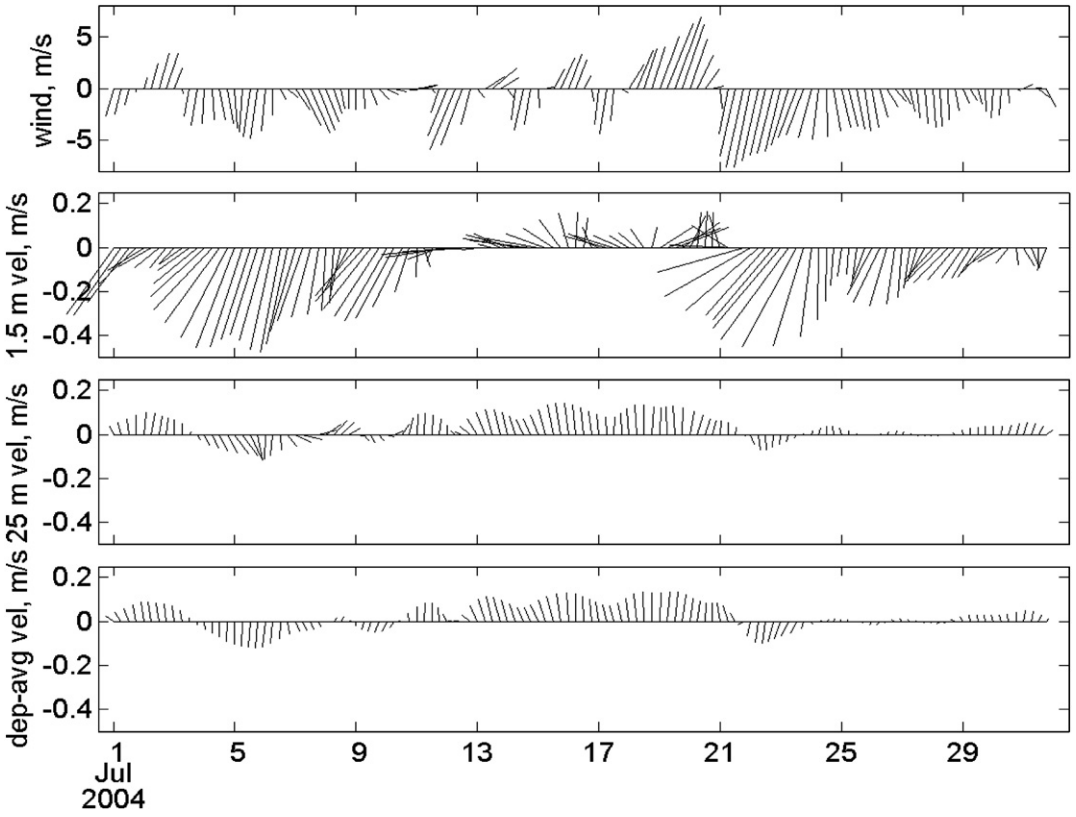

Fig. 4. 300 kHz ADCP current meter and wind times series for July 2004 for the central RISE mooring at 46 10.02° N 124 11.72° W, in 69 m water depth. Current data have been low-passed to remove tides; wind data have been filtered to remove diurnal sea breeze effects. From top to bottom: wind, currents at 1.5 m, currents at 25 m, and depth averaged velocity, all in m s^{-1}. Time on the x-axis is in calendar days, July 2004 (PST). See (Fig. 6b) for mooring locations.

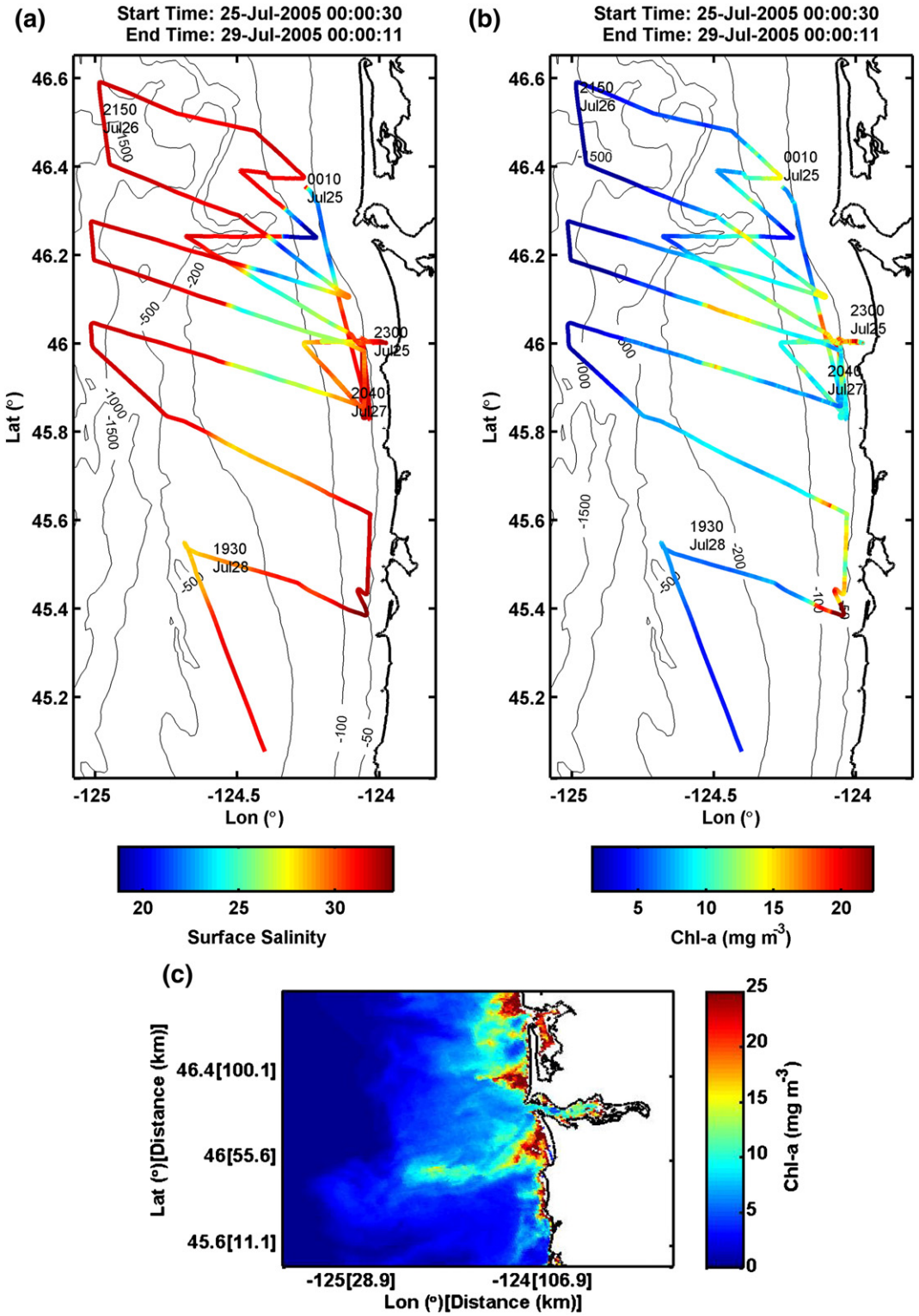

Fig. 5. Well-established upwelling: a map obtained 24–27 July 2004 of salinity (a) and Chl-a (b) at ~2 m depth during RISE-1. Data are from the *R/V Pt* UDAS; tides were weak. Plume waters have moved southward under the influence of sustained upwelling favorable winds. Upwelled waters are seen shoreward of the plume. MODIS-derived Chl-a (c) for 23 July 2004 at 2110 UT, ~8 h after high water (neap tide); Chl-a standing stock is generally low and mostly associated with plume waters.

System (CLASS) of National Oceanic and Atmospheric Administration (NOAA). Here, our use of the images involves rectification and editing to include only the relevant region near the mouth of the Columbia.

The ocean color data used here are from the Moderate Resolution Imaging Spectro-radiometer (MODIS) aboard an Aqua satellite, launched on 4 May 2002. Aqua MODIS views the entire Earth's surface every 1 to 2 days, acquiring data in 36 spectral bands. The MODIS ocean color data have been processed using O'Reilly et al. (1998) for chlorophyll a (Chl-a) and Van Mol and Ruddick (2005) for suspended particulate matter (SPM). To obtain concentrations of Chl a and suspended particulate matter (SPM), we used the normalized water leaving radiance (nLw) at bands of 412 nm, 443 nm, 488 nm,

531 nm, and 551 nm. The nLw data are available from: http://oceancolor.gsfc.nasa.gov.

4. Results: plume front dynamics

The asymmetries in frontal strength and internal wave generation defined in the introduction are a multi-scale problem, both conceptually and logistically, because the tidal plume (with its fronts and internal waves) is embedded within the plume near-field and the much larger plume far-field. The analysis in this section moves, therefore, from bulk-plume scales (described by remote sensing and vessel survey maps), to the tidal plume (described primarily by SAR images), to the tidal plume fronts and internal waves (described by SAR images and TRIAXUS sections). Regional context is provided by moored instrument data (Fig. 4). A dynamical explanation for the asymmetries described in this section is provided in the Discussion (Section 5).

4.1. Summer plume configurations

We begin by defining bulk plume configurations. The size and position of the bulk plume is related to the amount of Columbia River outflow, ambient currents, and coastal winds. There are four plume configurations that occur frequently during spring and summer in response to variable forcing (Hickey et al., 2005): upwelling (Figs. 2, 5a and b and 6a), weak and variable winds (with a tidal plume similar to that for upwelling winds; Fig. 1), downwelling (Figs. 3 and 6b), and bi-directional (combining features of Figs. 2 and 3). See Fig. 3 of Horner-Devine et al. (2009-this volume) for a conceptual view of plume configurations. Note that in terms of atmospheric forcing, there are only three states (upwelling-favorable, weak or neutral winds, and downwelling favorable). The bi-directional plume is a result of variable wind forcing over time, often after a period of elevated flow.

A typical example of summer winds and currents observed at a mooring in the plume area is shown in Fig. 4 for July 2004 (see Fig. 6a for mooring location). Light and variable winds (<5 m s^{-1}) prevailed until 17 July. This was followed by a brief downwelling episode 18–20 July with winds to 6 m s^{-1}, then persistent upwelling favorable winds as strong as 7 m s^{-1} on 21 July. While there is only a small disparity in the magnitude of the upwelling vs. downwelling-favorable winds, there is a much stronger difference in the currents at 1.5 m depth. Southward near-surface currents exceed 0.4 m s^{-1} on two occasions, while northward currents never reach 0.2 m s^{-1}. This disparity occurs only at the surface — at 25 m, currents are predominantly northward,

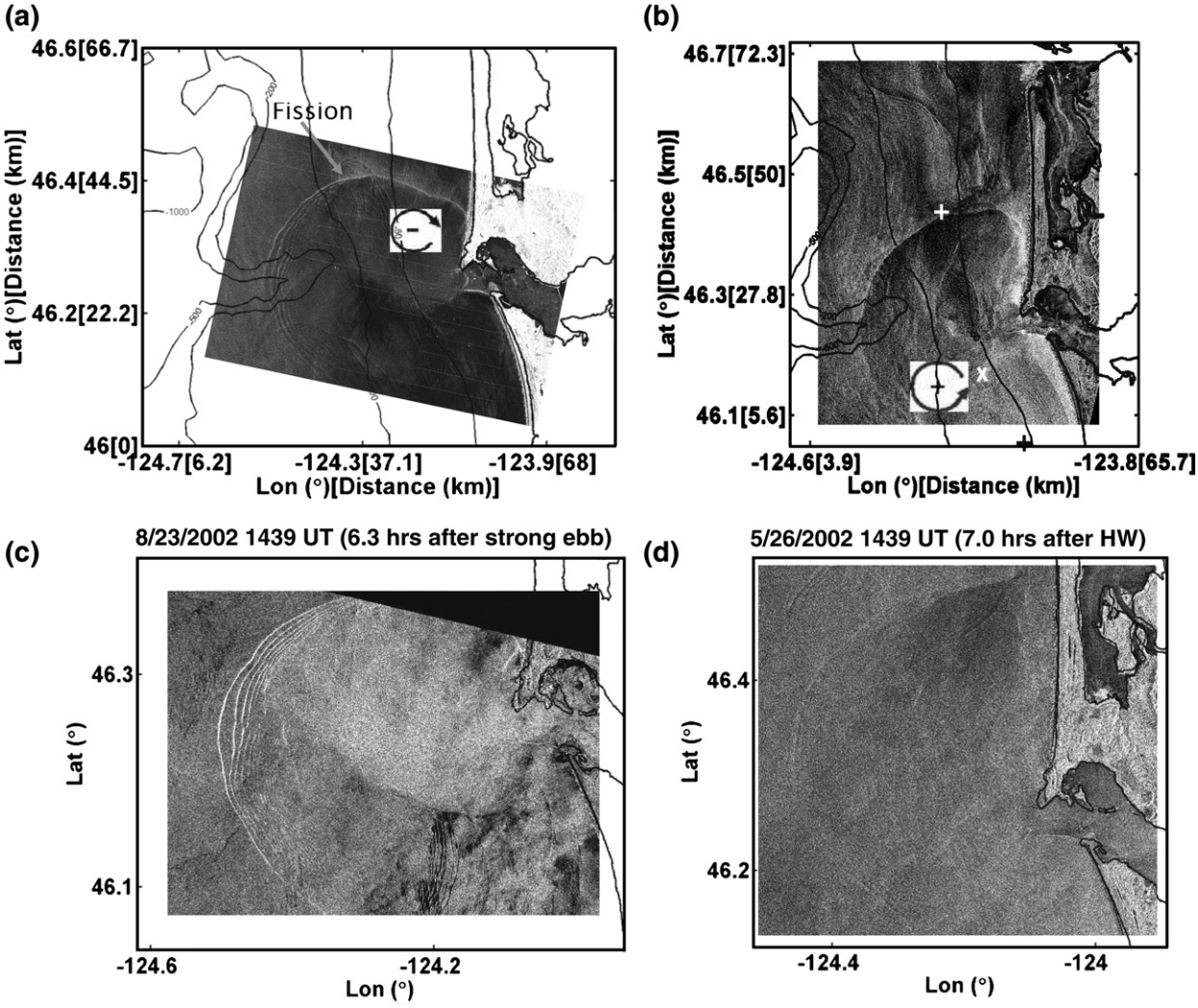

Fig. 6. SAR images for (a) upwelling (26 July 2004 at 1439 UT, 8 h after high water; a greater ebb with moderate tidal range) and (b) downwelling (24 May 2003 at 1439 UT, ~10 h after high water, a neap tide). Also shown for both cases is the hypothetical vorticity incurred by the upwind plume front in each case (see discussion in Section 5.1). In (a), there are 10–12 solitons visible on the west side of the plume. In (b) the upwind, S-SW quadrant of the tidal plume front has dissipated. Internal waves south of the river mouth, both inside and outside the tidal plume, appear to have originated in deep water and are propagating landward. The location of the 2005 RISE mooring data in Fig. 4 is shown by an *x* in (b); the other two mooring sites are shown by +. A typical strong soliton pattern (c) and a typical weak soliton pattern (d).

while depth-averaged currents show little predominance. The mooring shown in Fig. 4 is most representative of conditions in the plume near-field, but the other two RISE moorings show a similar (or larger) predominance of surface flow to the south; their locations are also shown in Fig. 6b.

Though there are four common summer bulk plume configurations and three forcing conditions, we focus here on upwelling and downwelling, because these two situations capture the frontal processes of interest. A typical plume configuration associated with prolonged upwelling is shown in Figs. 5a–c and 6a. These data were collected 24–27 July 2004; upwelling-favorable winds had persisted since late 20 July 2004 (Fig. 4). Columbia River flow at the most seaward gauging station (Beaver, 85 km from the ocean; waterdata.usgs.gov/or/) was 3600 to 4400 $m^3\ s^{-1}$ for 20–27 July 2004; tidal

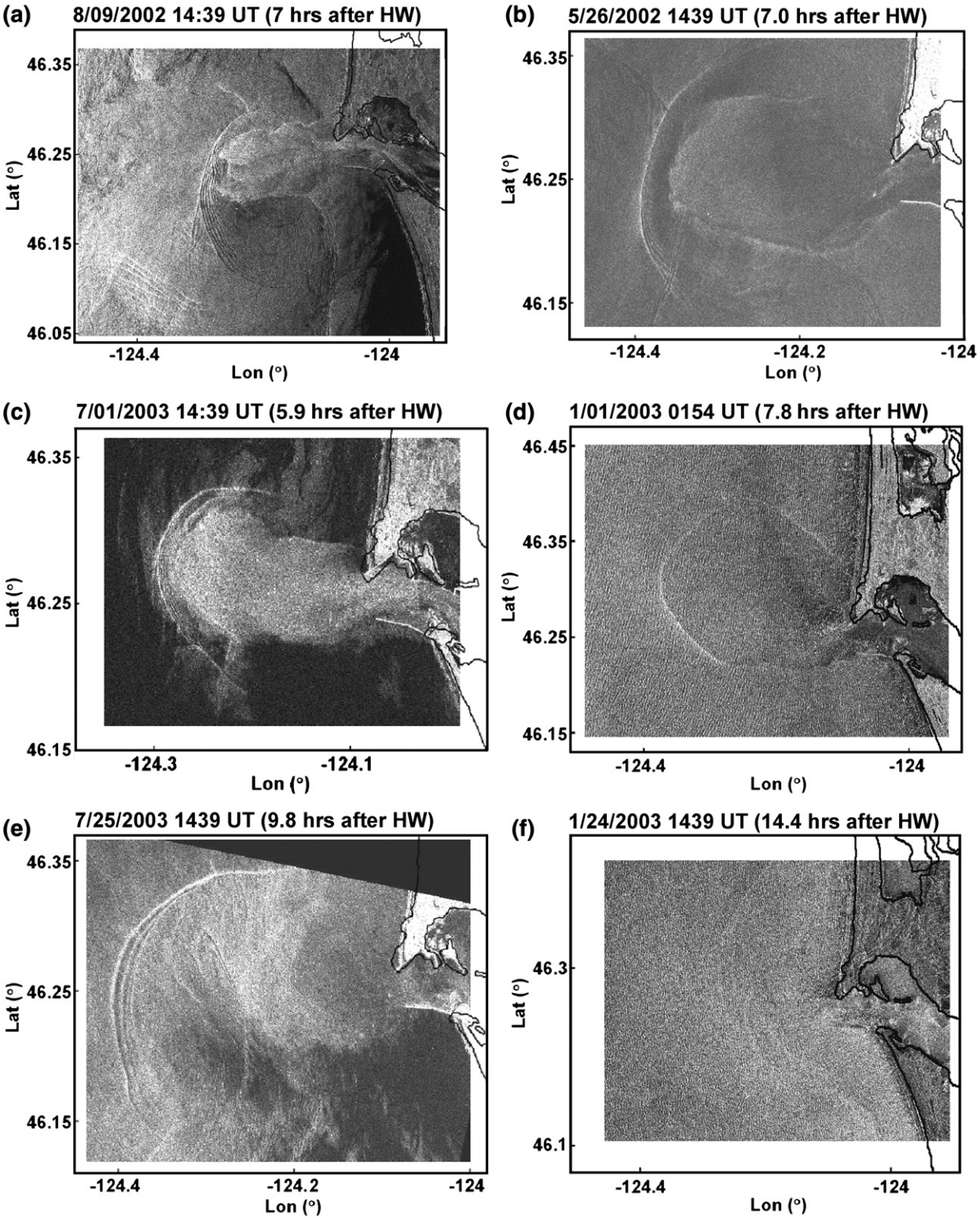

Fig. 7. Composite of four SAR images of tidal plume fronts during upwelling (left) and four for downwelling (right); HW = high water. All four upwelling fronts show internal wave generation, but only two downwelling fronts generated internal waves.

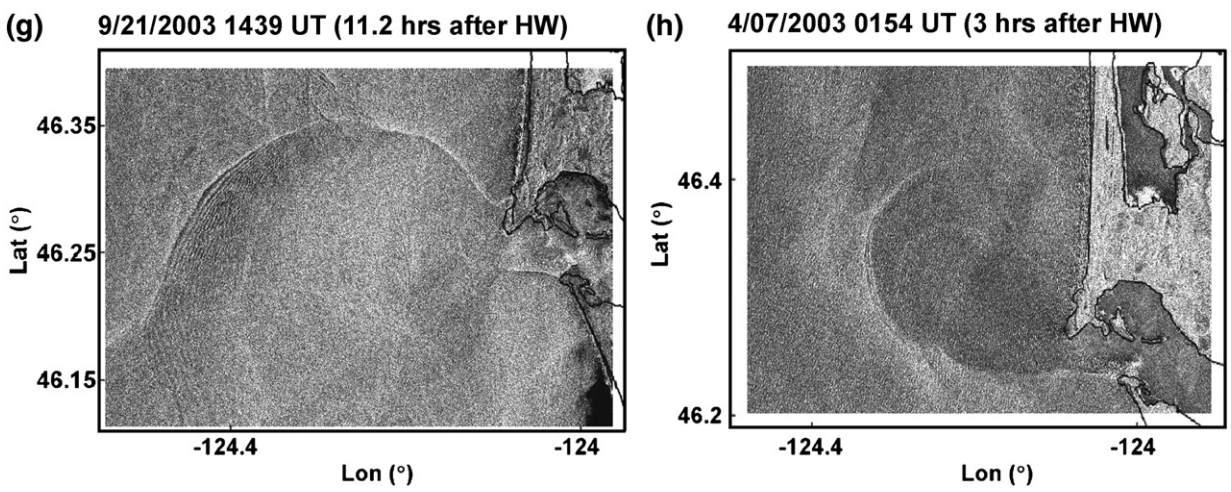

Fig. 7 (*continued*).

forcing was weak, 50–60% of the long-term average of 7300 $m^3\ s^{-1}$. The UDAS data in Fig. 5a show the plume moving southward and off the slope with $S<31$ water as far south as 45.3° N. Newly upwelled water ($S>33.5$) reaches the surface inshore of the new plume south of 46° N. High Chl-a levels are seen along the outer edge of the new plume to the north of the entrance and as its spreads offshore between 45.95° N and 46.2° N, and at the inshore end of several lines.

A MODIS-derived Chl-a map for 23 July 2004 shows high Chl-a levels (up to ~25 mg m^{-3}) and suggests strong productivity inshore of the plume, where some mixing of plume and upwelled water has occurred (Fig. 5c). There are also elevated Chl-a levels in a band extending offshore through the plume at about 45.85° N. A similar map for 22 July 2004, just after the onset of upwelling, suggests strong productivity around the margins of the plume, especially on its south side. Such Chl-a is likely the result of productivity associated with wind mixing of upwelled water into the plume as the plume bulge thinned and spread south into an area not occupied by the bulge the previous day (cf. Fong and Geyer, 2001). This interpretation is supported by a broad band of $T=12$–14 °C water on the 22 July 2004 SST map that corresponds to the higher Chl-a; new tidal plume waters had $T=15$–17 °C at this time (not shown).

The MODIS image does not define the tidal plume configuration, but Fig. 6a, a SAR image taken 26 July 2004, shows the corresponding tidal plume configuration. Note the strong tidal-plume front on the north side of the plume, where the plume is propagating into the oncoming flow, and internal wave generation has not yet taken place. There are at least six internal waves generated from a fission point that, given the propagation distances of the internal waves, has moved from south to north. These conditions are typical for upwelling.

Salinity and Chl-a for a typical bulk-plume configuration associated with downwelling are shown in Fig. 3. These observations were collected 18–20 June 2005 just before a spring tide and two days after a transition to downwelling favorable winds on 16 June 2004. Winds were weak and variable by the end of the map. River flow averaged 6400 $m^3\ s^{-1}$ and was decreasing slowly after the peak of the spring freshet on 20 May 2004 (~10,000 $m^3\ s^{-1}$). The lowest salinity water associated with the tidal plume water is directly offshore of the mouth at 45.25° N; new plume water has also moved northward between the 50 and 100 m isobaths. Moderate levels of Chl-a are associated with the plume bulge, north of the river mouth, but little Chl-a is being produced along the coast. The year 2005 was notable for the absence of sustained upwelling before mid-July. Under those conditions, the river and plume provides a significant part of the total (much reduced) production of Chl-a in the plume region. We do not have a SAR images for this time period, but a SAR image for similar spring flow levels in 2003 (Fig. 6b) shows a weaker front without internal wave generation. In fact, the front has dissipated entirely on its south (upwind) side. These conditions are typical for downwelling.

4.2. Occurrence of fronts and internal waves relative to forcing

Now consider tidal plume configurations for upwelling and downwelling in the context of the asymmetries mentioned in the Introduction. Fig. 7 includes eight representative SAR images (four upwelling and four downwelling) that show tidal plume fronts and/or plume-front generated internal waves. Fig. 7 conveys the idea that fronts are stronger under upwelling than downwelling conditions. Table 1 tabulates frontal properties in 52 SAR images for the 2001–2003 period for upwelling (winds predominantly to the south), 43 for neutral (winds not predominantly alongshore) conditions, and 34 for downwelling (winds predominantly to the north) conditions. Interestingly, Table 1 shows that it is primarily when the occurrence of weak fronts with internal waves is added to the occurrence of strong fronts that a difference between upwelling (and neutral) conditions is seen relative to downwelling conditions. The rationale for summing these two situations is as follows. Internal wave generation can remove as much as 75% of the total energy of a front (Pan and Jay, 2008), greatly reducing it advance speed into ambient water. We infer, therefore, that fronts that have released internal

Table 1
Summary for 2001–2003 of fronts observed in SAR images, by forcing condition.

Wind direction		Strong[a]	Weak w/ IW[b]	Strong + weak with IW	Weak[c]	Grand total
Upwelling	N&NW	8	14	22	8	30
(52 cases)	S&SW	4	0	4	2	6
	Both	3	1	4	2	6
	Total/%	15/29	15/29	30/58	12/23	42/81
Neutral	N&NW	3	8	11	1	12
(43 cases)	S&SW	5	1	6	7	12
	Both	4	2	6	1	7
	Total/%	12/28	11/26	23/53	9/22	32/74
Downwelling	N&NW	2	5	7	2	9
(34 cases)	S&SW	4	2	6	9	15
	Both	3	0	3	1	4
	Total/%	9/26	7/21	16/47	12/35	28/82
All forcing	N&NW	13	27	40	11	51
conditions	S&SW	13	3	16	18	34
(132 cases)	Both	10	3	13	4	17
	Total/%	36/27	33/25	69/52	33/25	102/77

[a] Strong: there is a narrow band of intense reflection.
[b] Weak with IW: a front is weak, but front-generated, seaward propagating internal waves appear.
[c] Weak: a front is visible but faint or diffuse.

Table 2
Summary for 2001–2003 of plume-front generated internal waves in SAR images, classified by wind forcing condition.

Cases	Strong[a] number/%	Weak[b] number/%	Total number/%
Upwelling (52 cases)	9/17	6/12	15/29
Neutral (43 cases)	4/9	7/16	11/26
Downwelling (34 cases)	2/5	5/11	7/16

[a] A SAR image is classified as having "Strong" internal waves when there is a clear, obvious internal wave pattern.
[b] A classification of "Weak" indicates that the internal wave pattern is faint or barely visible. Typical strong and weak solitons displayed in Fig. 6c and d.

waves were strong until their transition to subcritical condition and release of the waves. On this basis, upwelling and neutral conditions do more commonly show strong (or recently strong) fronts, but the difference is not huge.

There is a larger difference, however, in internal wave generation characteristics. Table 2 summarizes internal wave occurrence by forcing condition. (Fig. 6c and d show "Strong" and "Weak" internal waves, as used for classification in Table 2.) SAR images taken during upwelling and neutral conditions more commonly show front-generated internal waves (especially strong internal waves) than do downwelling images. In fact, only two downwelling cases show strong internal wave generation. This is important, because the rate of convergence at a front or internal wave "crest" is directly related to the strength of the SAR scattering cross-section — a stronger backscatter indicates a more energetic wave or front (Pan et al., 2007). Also, when internal wave generation is occurring, SAR images show a "fission point" — the location at which an internal wave is just leaving the plume front (cf. Fig. 6a). As further discussed in Section 4.6, the fission point always moves from south to north, un-zipping the front to produce non-linear internal waves. South-to-north fission is characteristic for all the internal waves captured in Fig. 7 and for almost all the SAR images summarized in Table 2, regardless of the sense of coastal forcing (upwelling, neutral or downwelling).

4.3. Upwelling frontal phenomenology and processes

We now examine the details of plume frontal propagation and internal wave generation by the tidal plume fronts, first for upwelling, then for downwelling. TRIAXUS sections taken on a neap tide, 13 June 2005, are typical for upwelling and neutral conditions (Figs. 8 and 9). The TRIAXUS section in Fig. 8 captures the initial fission of a northwestern front, ~5.6 h after high water. Fig. 9 shows a detail of a later stage of evolution of the internal wave train, starting 8 h after high water. A partial MODIS map for 13 June 2005 shows that the large-scale picture was similar to that shown in Fig. 2 for 29 May to 3 June 2005. The light northwesterly (upwelling-favorable) winds that began on 12 June 2005 were sufficient, in any event, to cause tidal plume fronts to behave in the manner similar to Fig. 6a. The prior week's river flow averaged 6800 $m^3\ s^{-1}$, down from a freshet peak on 20 May 2005 of 10,200 $m^3\ s^{-1}$ and 3000 $m^3\ s^{-1}$ below season average for mid-June.

The double depression in Fig. 8 represents a front (to the right at 124.314° W) and a newly spawned internal wave left of the front (at 124.318° W). The front, on the northwest side of the tidal plume, is propagating at 0.54 m s^{-1} into a relatively stratified plume bulge (Fig. 8b). High salinity, upwelled waters are found below 25–30 m. The front has become subcritical ($F_R = 0.4$) and has slowed after internal wave release. (Here, $F_R = U_f/(g'H_a)^{1/2}$ is the frontal F_R number, U_f is frontal speed, estimated by the velocity of plume water above a near surface stability maximum and relative to the

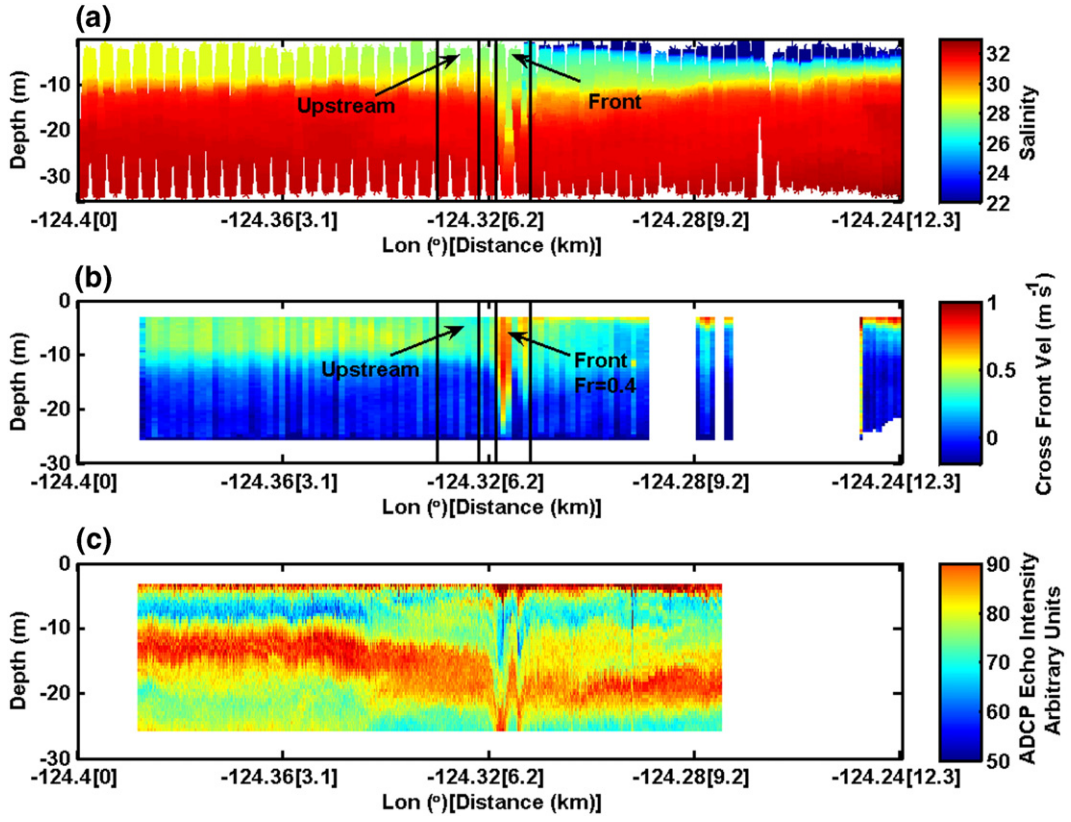

Fig. 8. Section showing internal wave fission from an upwelling plume front on 13 June 2005 1638 to 1941 UT; frontal crossing occurred at ~1810 UT, ~5.6 h after high water (neap tide). Shown are: a) salinity, (b) cross-frontal velocity in m s^{-1} from the 1200 kHz ADCP, with estimated internal F_R number, and (c) ADCP echo intensity corrected for absorption. The disturbance due to the front and internal wave penetrates to the bottom of the ADCP section at 25 m; salinity is perturbed to 35 m. Vertical lines define regions used for estimation of frontal and ambient (upstream) conditions.

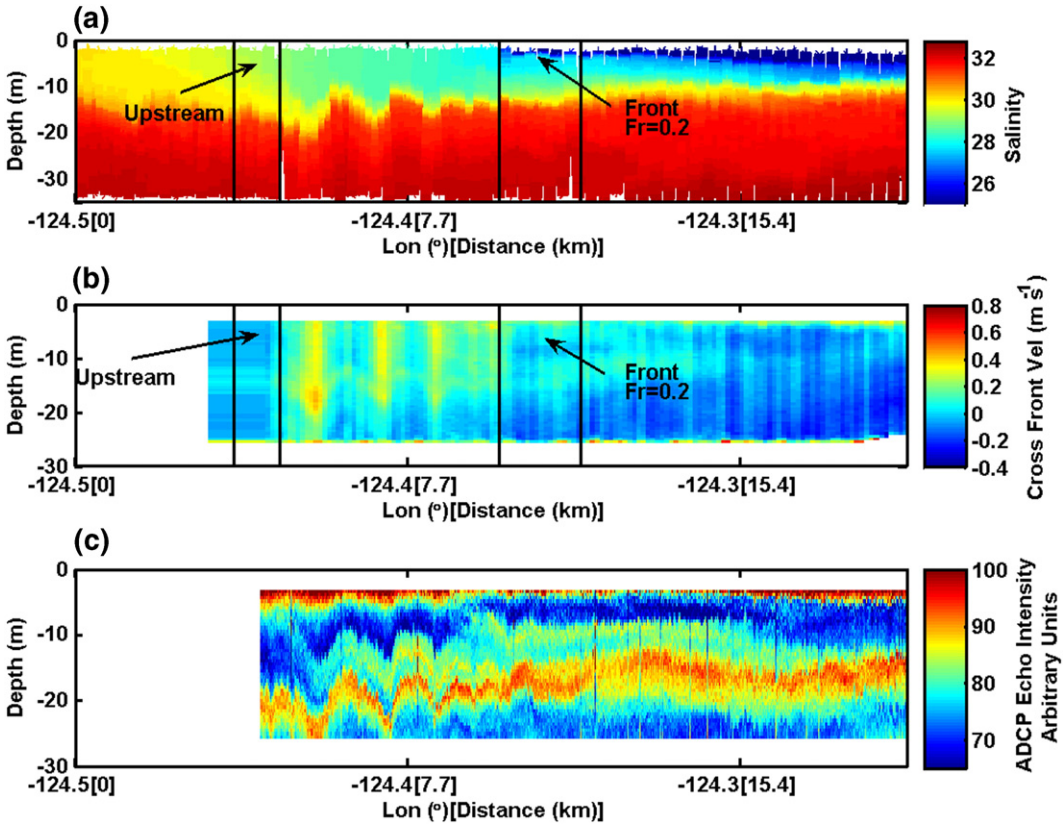

Fig. 9. Detail of internal wave movement away from an upwelling plume front. Shown are: a) salinity, b) cross-frontal velocity in m s^{-1} from the 1200 kHz ADCP, (c) ADCP echo intensity corrected for absorption. Data were collected during a 3-hour transect starting 13 June 2005 at 1947 UT; frontal crossing occurred at ~2100 UT, ~8 h after high water (neap tide). This captures a later stage in evolution of the soliton train than Fig. 8. Vertical lines define regions used for estimation of frontal and ambient (upstream) conditions.

oncoming flow, g' is reduced gravity in the ambient water, and H_a is the surface layer depth above a near-surface stability maximum in the ambient water. This discussion uses the same conventions as Nash and Moum, 2005.) The tidal plume is 6–10 m deep for several km behind the front at the time of fission, as judged by the depth of the $S=22$ contour (Fig. 8a). The front in Fig. 8 has moved >15 km (an average speed of ~0.74 m s^{-1}) in 5.6 h, remaining in a supercritical state until just before our sampling of it. For an upwelling front, this still constitutes an early transition to a subcritical state. The early transition is likely due to weak tidal forcing and high ambient stratification, the latter related to the recent high river flow levels.

Upwelling fronts are so sharp that their width is difficult to estimate from TRIAXUS data. At the front, there is a surface salinity difference $S>10$ between successive TRIAXUS profiles, ~200 m apart (Fig. 8a). The acoustic section (Fig. 8c) suggests that the frontal width (judged by the width of the plunge) is only 20–50 m. O'Donnell et al. (2008) argue that, from laboratory experiments, the width of coherent structures at the plume front should be $L_F=5\,\Delta U/N$, where: ΔU is the velocity difference between the plume layer and the underlying flow, and N is the buoyancy frequency. Based on this scaling, we expect a plunge width $L_F=$~20 m, which approximately accords with the width of the surface visual signal, but is smaller than the apparent plunge width by a factor of 2–2.5. When O'Donnell et al. applied this estimate to the Connecticut plume, they also found L_F to be too small by a factor of 1.5–2. A variety of factors may contribute to the discrepancy, including interaction with internal waves and 3-D frontal circulation.

CTD, velocity and acoustic data show that the sub-critical plume front is still energetic, despite the weak tidal forcing and prior release of an internal wave (Fig. 9). In terms of vertical motion, the plunge at the plume front affects the density field down to ~25 m. The first internal wave is even more energetic, penetrating to the bottom of the section at 33 m. Thus, despite the high stratification of the plume bulge area, plume fronts and the internal waves generated from them may potentially cause mixing down to the level of high salinity, upwelled water. This is often seen at around 30 m depth (e.g., in Figs. 8a and 9a).

Release of an internal wave train greatly alters frontal structure. The frontal crossing shown in Fig. 9 occurred 3 h after that in Fig. 8 (at ~2100 UT). The plume front is much broader (~2 km), has lost energy to the internal wave train, and has slowed to 0.13 m s^{-1} with $F_R=0.2$. Pan and Jay (2008) estimate that about 75% of kinetic plus available potential energy in a similar front was lost to internal wave propagation. The tidal plume has also shoaled with the $S=22$ contour at 6–8 m (Fig. 9a), while the pycnocline seaward of the front has deepened to a mean depth of ~12–13 m. There are four large internal waves between the front at 124.37° W and 124.45° W (Fig. 9b and c). The deepening of the pycnocline seaward of the front has likely occurred in part through the advection of plume waters seaward via a Stokes drift mechanism (Pan and Jay, 2008). The phase speed of such internal waves is O(0.6–0.8 m s^{-1}), slightly greater than the frontal speed at $F_R=1$. The lead internal wave can, therefore, move 5–10 km away from the front in the 3 h between the frontal crossings in Figs. 8 and 9, consistent with the position of these waves in Fig. 9. On stronger tides, more internal waves are released; e.g., >12 internal waves are visible in Figs. 6c and 7g (bottom left).

The observations shown in Figs. 7–9 are typical for upwelling fronts. They suggest the following picture of frontal processes under upwelling conditions; upwelling tidal plume fronts:

- Remain supercritical ($F_R>1$) for 6 to 12 h after high water, travelling 15–35 km from the river mouth before becoming subcritical.
- Are very sharp on the upwind (north) side of the river mouth, with a width of ~20 to 50 m.

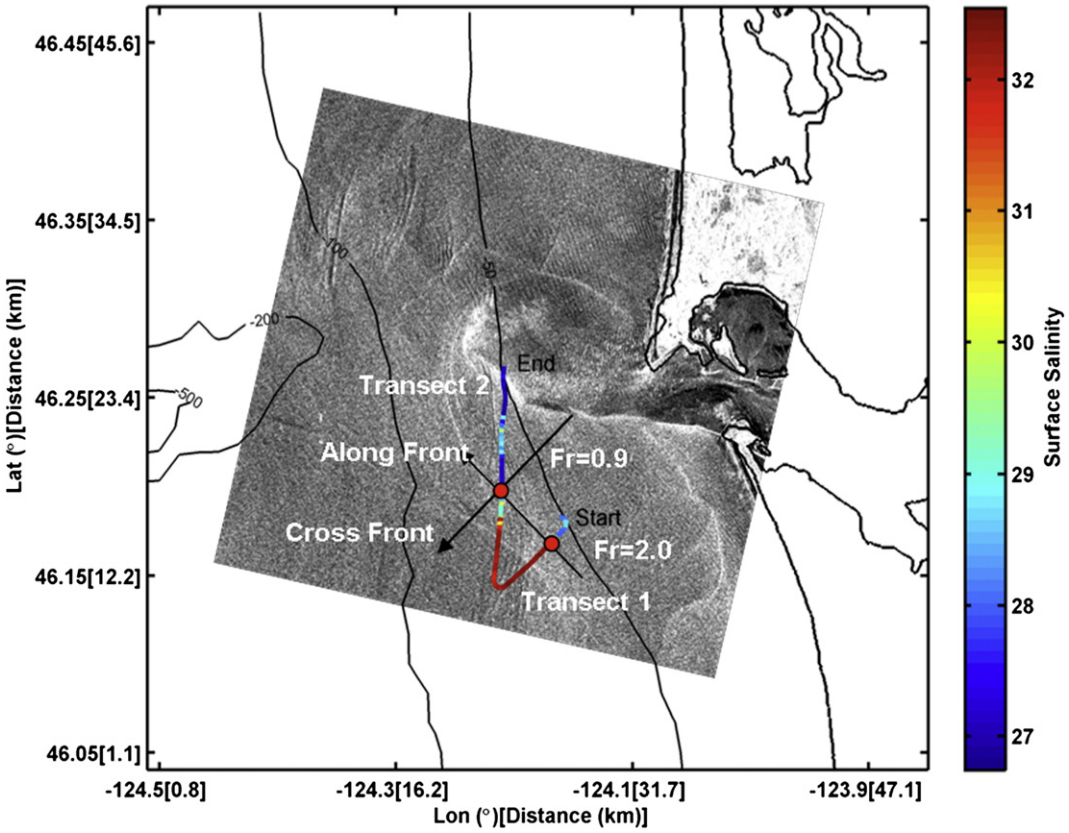

Fig. 10. SAR image taken 19 July 2004 at 1428 UT, about 5.5 h after high water under downwelling conditions (2 d after a spring tide), simultaneous with a TRIAXUS section. The *Pt Sur* UDAS salinity data overlaid on the SAR image were collected between 1322 and 1511 UT. The southern front is diffuse and deeper than upwelling fronts. There has been a transition between the time of the two transects from supercritical to subcritical conditions.

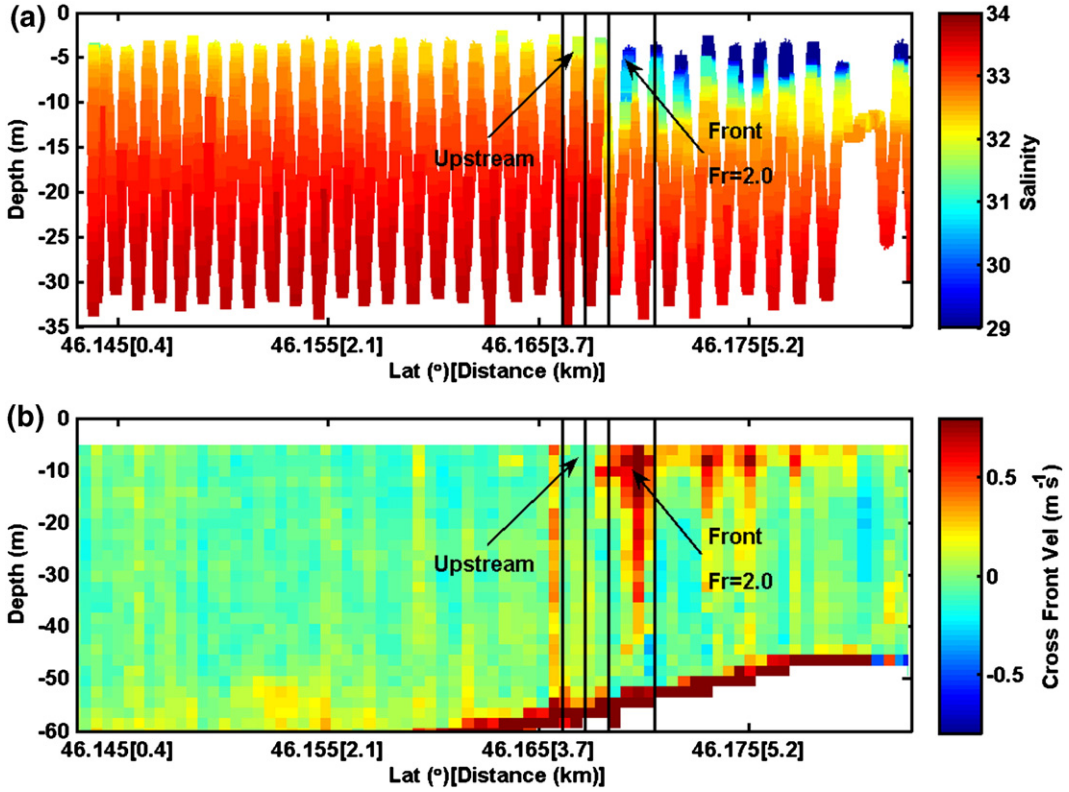

Fig. 11. Downwelling conditions: a TRIAXUS section corresponding to the first, more landward transect in Fig. 10; data were collected 19 July 2004, 4–5 h after high water (2 d after a spring tide). Shown are: (a) TRIAXUS salinity, and (b) across-frontal velocity as a function of depth, with the frontal Froude number F_R. F_R is calculated for the front relative to upstream conditions using the zones shown in (b). The entire frontal zone is wider than for upwelling, extending from ~46.166 to 46.172° N, >300 m.

- Bound a tidal plume that is shallower on its upwind side than during downwelling, are more energetic, and can accomplish more mixing than downwelling fronts (cf. Section 4.5).
- Are underlain by upwelled water (high in the nutrients, N and P) and surface ocean water. Thus, they should contribute to primary production more effectively than downwelling fronts, which overlie surface-ocean or old plume waters, both of which are nutrient depleted.
- Frequently spawn, upon transition to subcritical conditions, an energetic internal wave train that may contribute to mixing outside the plume and carries tidal plume water across the front (Pan et al., 2007).

An interpretation of these phenomena in terms of vorticity conservation is provided below.

4.4. Downwelling frontal phenomenology and processes

The observations used to describe typical summer downwelling frontal phenomena stem from 19 July 2004; a regional salinity map is shown in Fig. 3. This downwelling episode was brief (17–20 July), with peak poleward winds on 18 July of ~6 m s^{-1}. Fig. 10 shows a SAR image for 19 July 2004 at 1428 UT, 2 d after a spring tide. Superimposed on the SAR image are two 3 m salinity traces (from the *R/V Pt Sur* UDAS) across the frontal zone, covering the time period from 1322 to 1511 UT, ~4 to 6 h after high water. A moderately sharp front is seen at ~46.17° N in the earlier (more landward) of the two transects, but the second crossing of the frontal zone (covering the time of the SAR image) shows a diffuse frontal zone at ~46.2° N. Thus, a transition from supercritical to subcritical conditions has occurred between the times of the two transects. No seaward propagating internal waves were generated in the southern sector by this front, as is clear from the absence of such waves seaward of the front in Figs. 11 and 12. (There are several bands behind the main front in Figs. 10–12, and their origin is unclear.)

The TRIAXUS sections corresponding to the surface traces in Fig. 10 are shown in Figs. 11 and 12. The first section, the more landward of the two in Fig. 10, shows a well-defined front, ~300 m wide as judged from the salinity transition zone (Fig. 11a). The front is propagating at 0.59 m s^{-1} into nearly motionless (Fig. 11b), weakly stratified water. Total propagation distance over 4.5 h was ~15 km. There is a plunge defined by a single ADCP ensemble, which penetrates >30 m, deep enough to cause some mixing with high salinity, upwelled waters. The front is supercritical, with $F_R = \sim 2$. Between the times of Figs. 11 and 12, the plume deepened and became just subcritical ($F_R = 0.9$); its front is more diffuse. Also, the base of the plume (judged by the $S = 31$ contour) is at 8–14 m at right, deeper than in the upwelling case (compare Figs. 8a and 9a with Figs. 11a and 12a). After the transition to subcritical, the frontal speed has slowed to 0.14 m s^{-1} (Fig. 12b). A frontal plunge is barely visible in the ADCP record (Fig. 12b), affecting the flow only to about 12 m. Even though this is a spring tide and the sections were occupied before the end of the ebb (4–6 h after high water), the frontal zone is ~2 km wide (from ~46.167 to 46.2° N).

Clearly, the downwelling front in Figs. 10–12 is more diffuse than the upwelling front in Figs. 8 and 9. This situation is typical for downwelling conditions — upwind fronts during downwelling make an early transition to subcritical, usually without releasing internal waves. The absence of internal waves may be related to the low ambient stratification as well as to lower frontal energy levels. What is unusual about this pair of sections is that we were able to capture supercritical condition at all. Normally the transition to subcritical conditions occurs close to the estuary mouth, in an area too shallow for TRIAXUS observations. It is likely that an atypically long period of supercritical propagation occurred because of the large tidal range prevailing at this time.

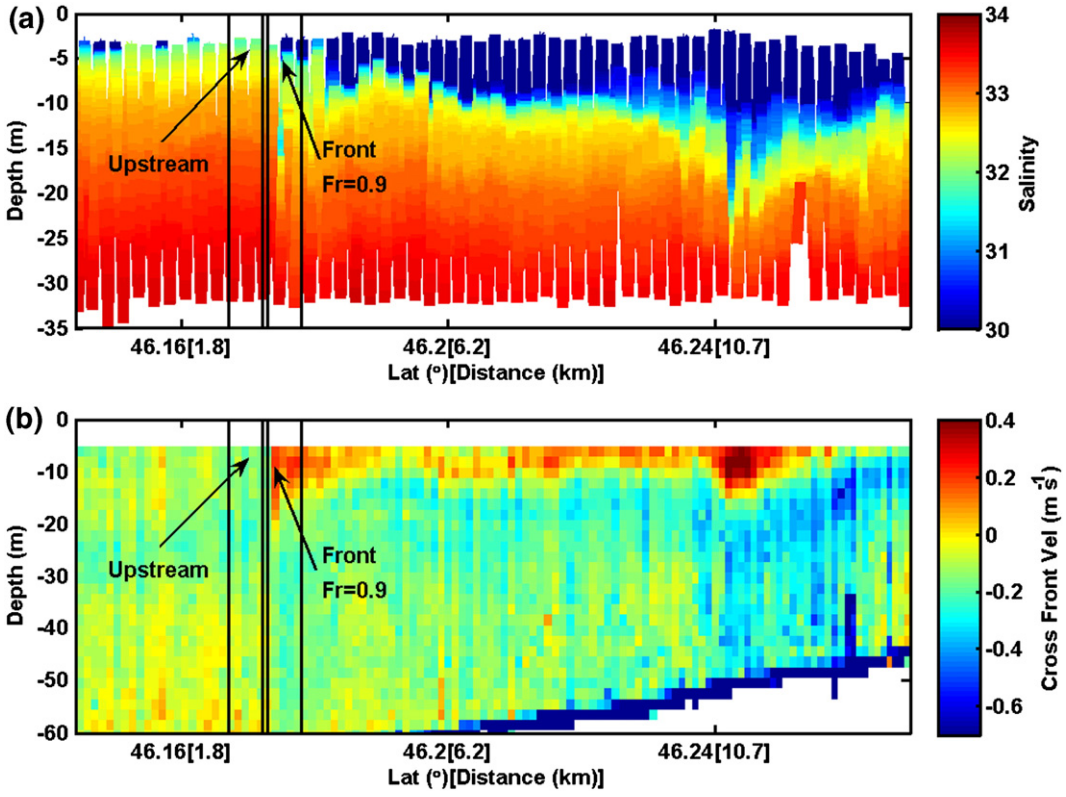

Fig. 12. Downwelling conditions: a TRIAXUS section corresponding to the second, more seaward transect in Fig. 10; data were collected 19 July 2004, 5–6 h after high water (2 d after a spring tide). Shown are: (a) TRIAXUS salinity, and (b) across-frontal velocity as a function of depth, with the frontal internal Froude number F_R. A transition from critical to subcritical conditions has occurred between the two sections. F_R is calculated for the front relative to upstream conditions using the zones shown in (b). The entire frontal zone is broad, extending from ~46.167 to 46.2° N, >2 km.

In summary, tidal plume fronts during summer downwelling conditions typically:

- Make an early transition to a subcritical state, <10–20 km from the estuary mouth, often before the end of ebb.
- Are, after transition, diffuse on the upwind (south) side, such that "frontal zone" is perhaps a better descriptor than "front".
- Are deeper on the upwind side than upwelling fronts, and cause less mixing (cf. Section 4.5).
- Usually do not spawn internal wave trains that contribute to mixing outside the plume.

4.5. Upwelling vs. downwelling differences in mixing

One method to evaluate the relative strength of mixing on the upstream side for upwelling and downwelling plume fronts is to examine plume layer properties for typical sections. Fig. 13 contrasts plume upper-layer depth H, upper-layer salinity S, and bulk Richardson number $Ri_b = \frac{g\Delta\rho H}{\Delta U}$ for the upwelling sections shown in Figs. 8 and 9 versus the downwelling sections in Figs. 11 and 12. (H is the depth of water above a near-surface stability maximum, and Ri_b is based on the velocity ΔU and density $\Delta\rho$ contrasts between the upper and lower plume layers.) Of the four sections, one occurs before (Fig. 11), and three after (Figs. 8, 9 and 12) the transition to subcritical. Especially in the section corresponding to Fig. 8 (just after the transition to subcritical conditions), the layer depth is smaller for the upwelling case, though layer depths are rather irregular for the downwelling case.

Only the section that corresponds to Fig. 8, for upwelling, shows a Ri_b value at or below critical level for suppression of mixing (~0.25) for any considerable distance, and then primarily on the plume side, where elevated mixing is expected. This same section shows a gradual increase in S over 4 km in a region where Ri_b is essentially critical, while H is actually decreasing in the direction of propagation. This suggests that plume spreading and mixing are both active, but that the mixing is not rapid enough to counteract spreading. The second upwelling section (for Fig. 9) shows an abrupt increase in S at the point of initial internal wave generation and then a gradual further increase in S in the seaward direction; H shows a slight thinning seaward of the fission point. If mixing is occurring seaward of the fission point, it may be due to a combination of internal wave and mean shear not reflected in our Ri_b, which is based on mean shear. The

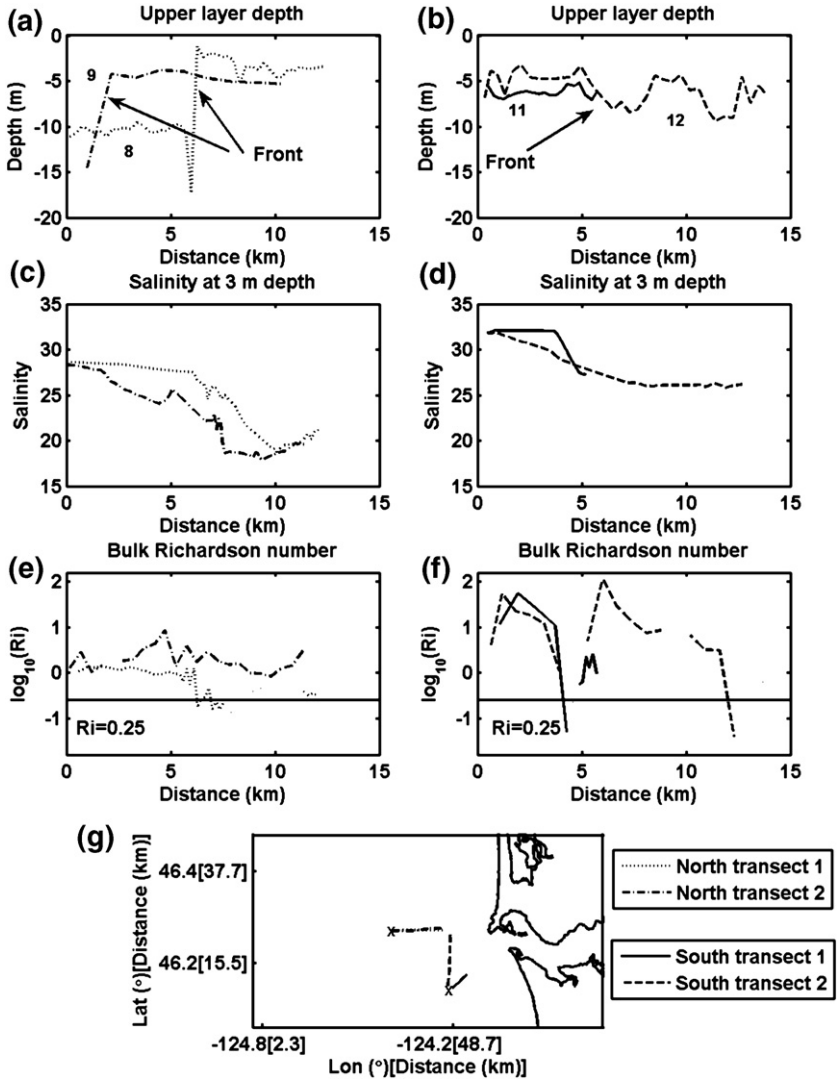

Fig. 13. A comparison of plume layer-averaged properties between upwelling and downwelling conditions: plume depth H for upwelling (a) and downwelling (b), salinity at 3 m for upwelling (c) and downwelling (d), bulk Richardson number Ri_b for upwelling (e) and downwelling (f), and (g) transect locations. The numbers in (a) refer to the figure showing the full section, Figs. 8 and 9 for upwelling and Figs. 11 and 12 for downwelling. The x-axis for (a) to (f) is distance in km along the transect from the location of the "x" in (g). See text for other details.

downwelling sections (for Figs. 11 and 12) show generally larger layer depths, $Ri_b > 5$, a gradual increase in S across the front, and a nearly constant S behind the front.

These salinity changes and layer depths strongly suggest that more mixing is associated with upwelling plume than downwelling fronts, and that internal waves are responsible for mixing beyond the plume front. The plume behind the downwelling fronts is also deeper. These features are consistent with potential vorticity control of frontal dynamics and internal wave generation described below in Section 5.1.

4.6. Asymmetry of internal wave generation

Sections 4.2–4.5 document tidal plume properties for various plume forcing conditions. Here, we examine internal wave generation by tidal plume fronts. Table 2 categorizes tidal plume-generated internal waves in SAR images by forcing condition (upwelling, neutral or downwelling). Internal waves generated at the tidal plume front are visible in 29% of the upwelling, 26% of the neutral cases, and 16% of the downwelling cases. Strong internal waves are seen in 17, 9 and 5% (respectively) of the upwelling, neutral and downwelling cases, emphasizing the more energetic nature of upwelling fronts. This predominance of strong internal wave generation under upwelling and (to a lesser extent) neutral conditions is consistent with the argument in Section 4.5 that these fronts are responsible for more mixing.

Not only is generation of internal wave trains by downwelling plume fronts less common than for upwelling and neutral fronts, but the direction of movement of the fission point does not change between upwelling and downwelling. In all upwelling and neutral cases and all downwelling cases for which the sense of frontal fission can be discerned, the front "unzips" from south to north. (There are two downwelling cases where the direction of unzipping is unclear, but that there are no confirmed examples for any forcing condition where the internal waves unzip from north to south.) This south to north unzipping is seen, for example, in the four upwelling cases in Fig. 7, as well as in the two downwelling cases with internal waves. In both of the downwelling cases, the front on the southerly side of the tidal plume has become indistinct by the end of ebb. The tidal plume front has unzipped from the southern quadrant to the northwest side, and an internal wave train is seen along the west side of the tidal plume.

In summary, when internal waves are generated by tidal plume fronts, the front first became subcritical on the south side of the tidal plume, leading to "unzipping" of the front from south to north. As argued in the next section, the most satisfactory explanation of this asymmetric internal wave generation is that the vorticity embedded in the emerging plume by the tidal outflow, not the strength and direction of alongshore currents, primarily controls the timing and location of internal wave generation from fronts.

5. Discussion and conclusions

5.1. A dynamical interpretation of tidal plume behavior in terms of potential vorticity

Analysis of tidal-plume potential vorticity conservation can be used to understand the asymmetric behavior of tidal plume fronts and internal waves. Potential vorticity is useful because it explains temporal changes in the frontal internal Froude number $F_R = U_f/(g' H_a)^{1/2}$ associated with the tidal plume, which governs internal wave generation. Consider conservation of potential vorticity $\Omega = (f+\xi)/H$ following a parcel of water (assumed vertically uniform) emerging from the estuary with the tidal plume front; $\xi = (\partial v/\partial x - \partial u/\partial y)$ is the vertical component of vorticity, f is planetary vorticity, and H is plume layer depth. The tidal stream (the ebb jet) seaward of the estuary entrance and alongshore coastal currents transfer vorticity to the nascent plume, altering its velocity and vorticity, and constraining the time and space variations of H. The results are different, however, for summer upwelling and downwelling situations.

Conservation of Ω and mass require for this emerging parcel of plume water:

$$\frac{D\Omega}{Dt} = \frac{D\left(\frac{f+\xi}{H}\right)}{Dt} = -\frac{1}{H}\nabla \times \frac{\vec{\tau}_i}{H\rho_0} \tag{5.1}$$

$$\nabla_H \cdot \cup_H = -\frac{1}{H}\frac{DH}{Dt} \tag{5.2}$$

Where: $\cup_H = \{u,v\}$ is the plume horizontal velocity, $\vec{\tau_i}$ is the interfacial stress vector, $\nabla_H = \{\partial/\partial x, \partial/\partial y\}$; x is onshore and y is alongshore, and ρ_0 is reference density. Assume for the moment that the plume is inviscid (unaffected by mixing) but that it takes on vorticity from the underlying tidal and coastal flows while still spreading radially due to its own buoyancy forcing. Changes in f over the tidal plume are also neglected as small. These assumptions are justified below using a scaling analysis, and effects of mixing are addressed. Because the analysis is inviscid, this analysis cannot be used to describe the highly non-hydrostatic plume front itself, where relatively strong mixing occurs. It is intended to apply to waters just behind the front.

The initial mid-channel condition at the plume lift-off point (where the initial value of H is set) is that $\xi_0 \cong 0$ because: a) $v = \partial v/\partial x \sim 0$ (the flow is straight west [with $u<0$] and axially non-divergent in a jetty-constrained channel of nearly constant width and depth), and b) $\partial u/\partial y = 0$ in mid-outflow because the tidal outflow is strongest in mid-channel. Once the plume has left the estuary, there is lateral shear in the jet-like ebb outflow (Chao, 1990). Specifically, $\partial v/\partial x < 0$ and $\partial u/\partial y > 0$ north of the channel centerline (so that ξ decreases), while $\partial v/\partial x > 0$ and $\partial u/\partial y < 0$ south of the channel centerline (so that ξ increases).

Now consider near-frontal water parcels on the upwind side of the river mouth for upwelling and downwelling conditions; see Fig. 6a and b for a conceptual view of plume potential vorticity:

- Upwelling: the winds are from north to south, and the upwind front is to the north of the river mouth. The upwind front remains supercritical ($F_R > 1$) for ~6–12 h after high water, with a sharp front (Section 4). For water in a northward turning plume front, the spreading and anticyclonic rotation of the tidal outflow causes ξ to decrease ($\xi < \xi_0$; Fig. 6a). The scale of the tidal plume (<25 km) is small enough that changes in f are small relative to those in ξ. Therefore, H must decrease to conserve Ω (Eq. (5.1)), maintaining rapid seaward movement of the front. From Eq. (5.2), the plume spreading necessary to decrease H can occur both by axial and lateral divergence. Given any fixed density contrast, the small H and high velocity will raise the frontal Froude number F_R. The front stays sharp because waves cannot propagate away from it. Frontal energy is eventually lost by a pulse of internal wave generation (Nash and Moum, 2005), but this typically occurs after the end of ebb, well into the following flood. The coastal flow contributes to frontal convergence, and more strongly during upwelling than downwelling, because the oncoming coastal flow for upwelling conditions is usually larger during the summer season considered here — it may reach 0.4 m s^{-1} at the surface (Fig. 4).
  The vertical density contrast between plume waters and the underlying flow also affects F_R in a different way during upwelling vs. downwelling. Upwelling pushes old plume water away from the coast, replacing it by high salinity (S), low temperature (T) upwelled water, yielding a high initial value of g' beneath the plume. This initially high value of g' does not, however, preclude supercritical conditions from occurring at the plume front, and variations in U_f

dominate evolution of F_R near the front (Nash and Moum, 2005). Moreover, to the extent that mixing occurs, it reduces g' more during upwelling than downwelling, helping to maintain $F_R>1$. When the plume eventually becomes subcritical, it usually generates internal waves. However, internal wave generation from the north side of the plume is sometimes limited during upwelling by low ambient stratification.

- Downwelling: the winds are from south to north, and the upwind front is to the south of the river mouth (Fig. 6b). The upwind front becomes subcritical ($F_R<1$), broad and diffuse within a few hours after it leaves the estuary. For the waters in the upwind front (i.e., in waters that turn southward), the spreading and cyclonic rotation of the ebb jet cause ξ to increase ($\xi>\xi_0$; Fig. 6b), H must also increase. From Eq. (5.2), lateral spread (plume divergence) must be compensated by axial convergence to satisfy Eq. (5.1), slowing the front. Given any fixed density contrast, low frontal velocity and high H will both lead to a low value of F_R, even if the initial density contrast is less than in the upwelling case. The front is diffuse, because the front becomes sub-critical at an early point in its propagation, and energy can propagate away from it. Downwelling traps old plume water near the coast, reducing the initial g', but not usually enough to allow the plume front to be supercritical ($F_R>1$) through the entire ebb (6 h). Whatever the initial density contrast, it is not greatly altered by mixing before the end of the relatively brief supercritical phase.

A scaling argument using representative velocities makes the above changes in vorticity clearer. The initial value of planetary vorticity f for a plume at 45 N is $\sim 1.2\times10^{-4}$ s^{-1} The maximum absolute change in f over 20 km (a typical radius for a fully developed tidal plume) is $\sim 5\times10^{-7}$ s^{-1}, small enough to be neglected. The initial boundary condition requires that $\xi \sim 0$ for water in mid-channel. The change in relative vorticity $\xi=(\partial v/\partial x-\partial u/\partial y)$ implied by the initial turning of the plume from directly offshore (with $U\sim-1.5$ m s^{-1} and $V=0$) to northward ($U=0$, $V\sim0.75$ m s^{-1}) over half the above radius (12.5 km) is $\xi=(\partial v/\partial x-\partial u/\partial y)\sim-0.6\times10^{-4}$ s^{-1}, yielding $f+\xi=0.6\times10^{-4}$ s^{-1}. The subsequent turning of the water near the front as it moves back onshore and begins to rotate ($U\sim0.5$, $V\sim0.5$ m s^{-1}) ~25 km north of the entrance yields $\xi=(\partial v/\partial x-\partial u/\partial y)\sim-0.8\times10^{-4}$ s^{-1}, reducing $f+\xi$ to 0.4×10^{-4} s^{-1}, 1/3 its initial value.

Further, for an initial $\xi\sim0$ and a typical plume lift-off depth of ~8–10 m, the initial ~50% decrease in $f+\xi$ (to $\sim0.6\times10^{-4}$ s^{-1}) for water parcels moving north during upwelling cannot be fully balanced by changes in plume depth (which are typically still 6–8 m at this stage), because this would require a plume of only ~3 m depth. Dissipation is important during initial tidal plume movement, and thinning of the plume is counteracted by mixing and increased salinity. The latter evolution of plume waters (which caused in our example a further drop in $f+\xi$ to $\sim0.4\times10^{-4}$ s^{-1}) is more closely balanced by changes in plume depth, which is typically 3–6 m at this stage.

Changes in ξ during downwelling are not exactly opposite to those for upwelling, because of rotation and coastal currents. A water parcel originating near mid-channel and moving southward behind the plume front during downwelling would incur an increase in $f+\xi$ to $\sim2\times10^{-4}$ s^{-1}, requiring (for potential vorticity conservation) a thickening of the plume that is not observed — the plume remains close to its initial thickness (~8 m) as it spreads and mixes. As is also the case for the northern plume front, the torque associated with plume dissipation opposes the changes in potential vorticity implied by the imparting of ξ to the plume by the tides. Thus, the southern plume front is deeper than the northern one, but not as deep as this inviscid argument would make it. Clearly, mixing (not considered in the above scaling) alters frontal propagation, e.g., by limiting the speed of frontal movement. Nonetheless, there is ample precedent to suggest that an inviscid analysis can provide a lowest-order explanation of important bulk plume properties (e.g., Yankovsky and Chapman, 1997; Horner-Devine, 2009).

Scaling also justifies use of an inviscid analysis; i.e., neglect of the right hand side of Eq. (5.1). The above values of ξ suggest a $\frac{D(\xi/H)}{Dt}10^{-9}$m^{-1}s^{-2}, assuming $H\sim5$ m and a 6 h propagation time. Taking eddy and mass diffusivities $K_m\sim K_\rho\sim10^{-3}$–$10^{-4}$ behind the front (Orton and Jay, 2005), we estimate the neglected stress curl term [on the right in Eq. (5.1)] as 10^{-10} to 10^{-11} m^{-1} s^{-2} for water masses just behind the front.

Further, we should consider the implications for tidal plumes during neutral and variable (light) wind circumstances. Our analyses of SAR images suggest that the tidal plume and its fronts behave under neutral and variable (low) wind conditions very much as they do during upwelling. This is not surprising, because the California current imposes a bias toward equatorward alongshore currents in summer (Hickey, 1989). Equatorward currents are weakened by neutral winds but do not altogether disappear, at least not in summer. There is, however, one important difference between the upwelling and neutral cases — during low winds, mixing by plume fronts is unlikely to mix high-nutrient, newly upwelled waters into surface waters.

Finally, our analysis can be tested by examining north–south sections across the plume before the transition to subcritical conditions. These show that the tidal plume is indeed deeper on the south side; see Fig. 14 and Figs. 5 and 6 in Horner-Devine et al. (2009-this volume), all for relatively weak winds. (It is necessary to confine this test of the vorticity hypothesis to the period of critical propagation. After that time, the transition of the southern plume front to a subcritical state allows thinning of the southern frontal area, as is seen in Figs. 8 and 9 of Horner-Devine et al., 2009-this volume) The observations of the Connecticut River plume by O'Donnell et al. (1998) show a similar decrease in plume depth for waters with a more negative vorticity (judged by their position). Because the Connecticut plume always turns left with the ebb in Long Island Sound, it is not possible to compare upwelling and downwelling plumes for that system.

5.2. Tidal plume fronts and internal wave generation

Tidal plume fronts play a vital role in mixing of plume waters into the bulk plume, and in nutrient supply to the plume. Strong mixing occurs much of the way around the periphery of the tidal plume, presumably anywhere the plume is supercritical. Mixing occurs in association with frontal passage and, after internal wave release, due to the combination of mean and internal wave shear (Pan et al., 2007). Internal wave generation is common during upwelling and neutral periods with cross-shore winds, but much less common during downwelling periods.

The Nash and Moum (2005) analysis and the results discussed here suggest that, for internal waves to form, a front must be initially super-critical, with strong frontal convergence causing formation of a bore head. A sub-critical front will lack the energy to release internal waves. The stratification of the ambient ocean outside the plume front is also vital, however, and this is one reason that the plume region is so rich in internal waves. The ocean on the seaward side of the front must be stratified (but not too stratified) such that the propagation speed for nonlinear internal waves is less than the initial plume propagation speed, but greater than the intrinsic (linear wave) propagation speed of the stratified coastal ocean. Furthermore, internal wave formation modulates the strength and propagation of fronts. The strongest fronts on the north side of the front during upwelling conditions maintain rapid propagation for up to 12 h past high water. They usually spawn internal waves, except when the plume lies over unstratified, high-salinity upwelled water where such waves cannot propagate. These internal waves both transport freshwater across the initial plume front and propagate energy seaward. This energy may cause mixing outside the immediate plume bulge (Pan and Jay, 2008). Thus, plume fronts

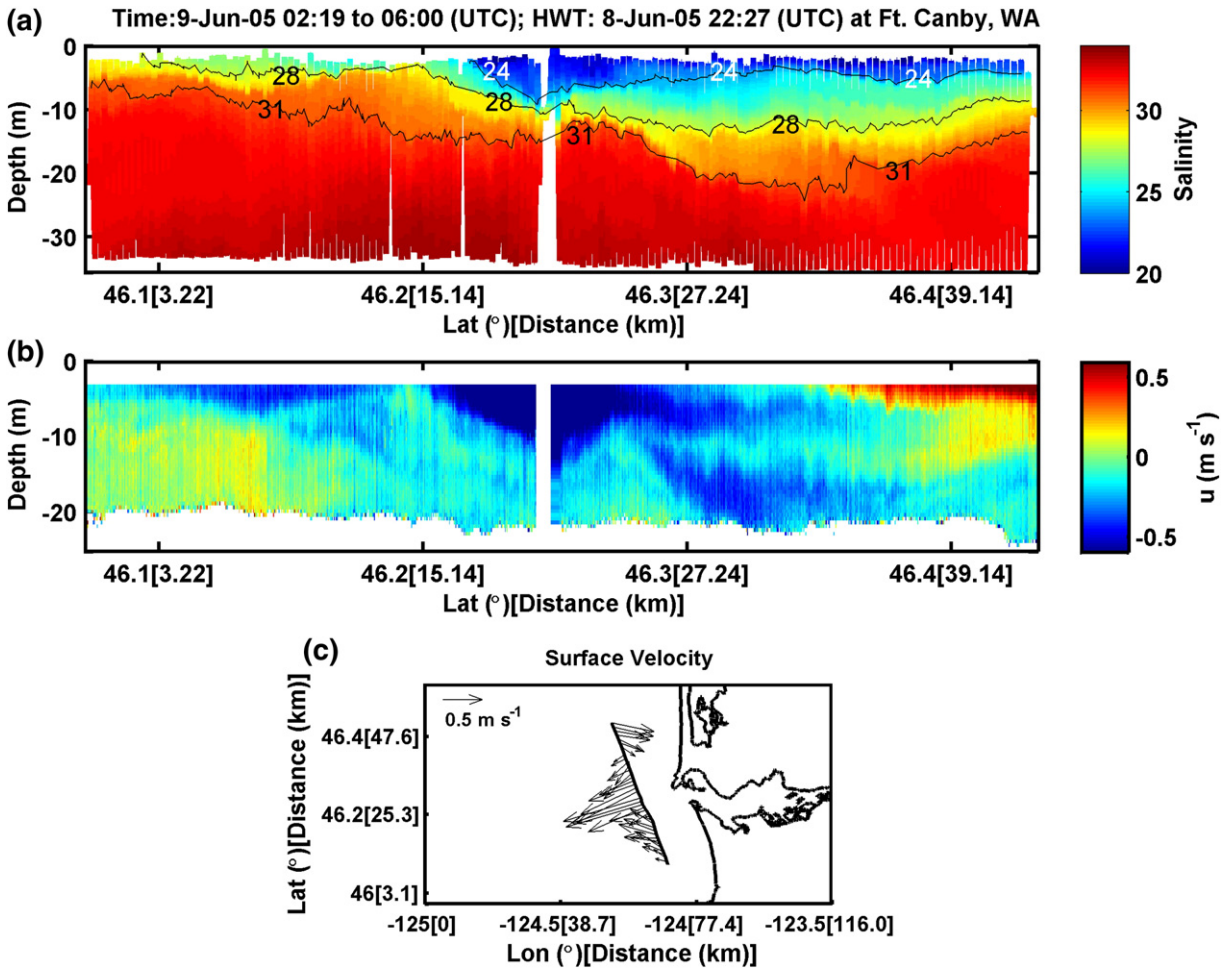

Fig. 14. A section across the tidal plume taken 9 June 2005 starting at 0219, ~4 h after high water; river flow varied from 7800 to 9200 $m^3\ s^{-1}$ over the previous week. Shown are: in (a) a salinity section, (b) an east–west velocity section, and (c) surface velocity components. The contours in a) are from surface down, $S = 24$, $S = 28$ and $S = 31$, denoting the upper limits of the tidal plume, plume bulge and plume far-field. Note the thickening of the tidal plume to the south.

and internal waves play an important role in plume and regional productivity.

5.3. Tidal plume fronts and coastal primary production

Section 4 suggests that frontal processes and internal waves drive strong mixing that contributes to high productivity around the margins of the plume near-field. This mixing and its impact on productivity are strongest on the west and northwest sides of the plume (and sometimes also the north side), because:

- The vorticity transferred to the tidal plume by the ebb outflow makes these fronts very energetic, causing the most mixing within the tidal plume and releasing the most energy in the form of internal waves to facilitate mixing within the rest of the plume bulge.
- Strongly supercritical fronts occur preferentially during upwelling conditions when nutrients N and P are available from upwelled water to be mixed with plume Si and Fe.

These two factors suggest that the entire plume near-field should be quite productive, especially north of the river mouth. Indeed, enhanced nutrient supply related to tidal-plume-induced mixing may be one factor causing the Washington shelf to exhibit higher primary productivity and standing Chl-a stock than the Oregon shelf, despite generally stronger upwelling off Oregon. However, Chl-a levels are often larger around the boundaries of the tidal plume than directly in a new ebb outflow — even if productivity is high, accumulation of sufficient standing stock to yield high Chl-a values takes some hours (Horner-Devine et al., 2009-this volume). Thus, a new ebb outflow may exhibit low Chl-a values even as nutrients are being mixed into it.

Ocean color images and other data suggest that the outer part of the tidal plume and plume near-field are quite productive under upwelling, neutral and transitional conditions. Modest productivity is sometimes found even during downwelling. Examination of 56 ocean color images for 2004 to 2005 suggests, however, that productivity associated with the plume is not always on the west, northwest and north sides (e.g., Fig. 6). The mechanisms discussed here enhance productivity on the west, northwest and north sides of the plume during steady upwelling. Other parts of the plume near-field may experience enhanced mixing and productivity whenever the plume is strongly transient, especially in the offshore direction — as suggested by Fong and Geyer (2001), plume advection by shifting winds causes thinning of the plume and mixing.

This high productivity, and the vertical mixing on which it is based, occur despite high stratification. Indeed, the mixing induced by fronts and internal waves is part of the "paradox of plume mixing" — mixing occurs through mechanisms (supercritical fronts and internal wave generation) that exist only in a stratified environment. Furthermore, productivity is enhanced by the fact that the plume is the active layer in near-field mixing, so that entrainment into the tidal plume predominates, and the tidal plume maintains its identity for a sufficient length of time to allow photosysnthesis to take place in what is analogous to a shallow mixed layer. Locally, the strength of mixing or entrainment can be expressed in terms of a Richardson number — a ratio of buoyancy to stratification (e.g., Souza and Simpson, 1997). However, a parameterization of plume-related mixing (by both fronts and internal waves) in

terms of the bulk plume properties (e.g., river discharge, estuary mouth width and initial density difference) is lacking.

5.4. Salmonids and the seasonality of plume processes

There is an important connection between the plume mixing processes discussed here and survival of the Pacific Northwest's endangered salmonids. Persistent upwelling typically begins in late June (Hickey, 1989), and the seasonal timing of upwelling has changed little over time, at least as judged by the timing of the spring transition (Logerwell et al., 2003). Though some out-migration occurred throughout the year, the largest number of juvenile salmonids also came downstream in late June and July (Bottom et al., 2005), just in time to utilize secondary productivity based on upwelled nutrients. Historically, this out-migration was associated with the spring freshet; now it is set by hatchery schedules.

A striking change has taken place in the Columbia River flow cycle over the last 125 years (Bottom et al., 2005), de-synchronizing it with the onset of upwelling and salmonid behavior. The peak river flow has shifted from late June prior to 1900 to late May. The freshet continues to migrate to earlier dates, because of an earlier snow melt and human alteration of the flow cycle. Moreover, the average and freshet peak flows have decreased ~15% and >40%, respectively, mostly due to human factors. Thus, before 1900, a large freshet peak typically occurred in late June about the same time as the onset of strong upwelling. This combination of high river flow and strong upwelling provided high levels of N, P, Si and micronutrients to the plume area and Oregon and Washington shelves. The frontal processes discussed here facilitated mixing of plume and upwelled nutrients. Moreover, colder water temperatures and the shorter residence time of water in the historical river (without dams) likely caused the system to provide more nutrients to coastal waters than at present (Small et al., 1990). Thus, even if the largest historic freshets suppressed mixing for a time, productivity could have been supported by plume nutrients (cf. Fig. 2).

High levels of primary productivity (and the secondary production it supported) during and after the spring freshet must have provided seaward migrating juvenile salmonids with an ample food source. Also, the higher historic sediment load (at least double modern levels; Bottom et al., 2005) associated with larger historic freshets provided juvenile salmonids with protection from predation (Pearcy, 1992). While a full understanding of the support of salmonid survival by the coastal ecosystem remains elusive, the growing mismatch between the peak river flow (now late May) and the onset of upwelling and the peak of the juvenile salmonid migration (late June) may limit the ability of the coastal ocean to support juvenile salmonids.

Acknowledgements

This research was funded by the Bonneville Power Administration and NOAA-Fisheries (project: Ocean Survival of Salmonids), and the NSF (project RISE — River Influences on Shelf Ecosystems OCE 0239072). Thanks to Ed Dever of Oregon State University for the current meter data in Fig. 4. We also thank Captain Ron L. Short of the *R/V Pt Sur* and Marine Technicians Stewart Lamberdin, Christina Courcier, and Ben Jokinen for their superb support of in-situ data collection. The SAR images were provided by Comprehensive Large Array-data Stewardship System (CLASS) of National Oceanic and Atmospheric Administration (NOAA). Thanks to Nate Mantua and Alan Hamlet of the University of Washington for discussion of the connection between salmonid survival and freshet timing.

References

Barnes, C.A., Duxbury, C., Morse, B.-A., 1972. Circulation and selected properties of the Columbia River plume at sea. In: Pruter, A.T., Alverson, D.L. (Eds.), The Columbia River Estuary and Adjacent Ocean Waters. University of Washington Press, Seattle, WA, pp. 41–80.

Bottom, D.L., Simenstad, C.A., Burke, J., Baptista, A.M., Jay, D.A., Jones, K.K., Casillas, E., Schiewe, M.H. 2005. Salmon at river's end: The role of the estuary in the decline and recovery of Columbia River salmon. U.S. Dept. of Commerce, NOAA Tech. Memo., NMFS-NWFSC-68, 246 pp.

Chao, S.-Y., 1988. Wind-driven motion of estuarine plumes. J. Phys. Oceanogr. 18, 1144–1166.

Chao, S.-Y., 1990. Tidal modulation of estuarine plumes. J. Phys. Oceanogr. 20, 1115–1123.

Cudaback, C.N., Jay, D.A., 1996. Buoyant plume formation at the mouth of the Columbia River — an example of internal hydraulic control? In: Aubrey, D.G., Friedrichs, C. (Eds.), Buoyancy Effects on Coastal and Estuarine Dynamics. AGU Coastal and Estuarine Studies, vol. 53. American Geophysical Union, Washington, DC, pp. 139–154.

Cudaback, C.N., Jay, D.A., 2000. Tidal asymmetry in an estuarine pycnocline: I. Depth and thickness. J. Geophys. Res. 105, 26,237–26,252.

Fong, D.A., Geyer, W.R., 2001. Response of a river plume during and upwelling favorable wind event. J. Geophys. Res. 106, 1067–1084.

Fong, D.A., Geyer, W.R., Signell, R.P., 1997. The wind-forced response of a buoyant coastal current: observations of the western Gulf of Maine plume. J. Mar. Sys. 12, 69–81.

Garcia-Berdeal, Hickey, B.M., Kawase, M., 2002. Influence of wind stress and ambient flow on a high discharge river plume. J. Geophys. Res. 107, 3130. doi:10.1029/ 2001JC000392.

Garvine, R.W., 1982. A steady-state model for buoyant surface plume hydrodynamics in coastal waters. Tellus 34, 293–306.

Hickey, B.M., 1989. Patterns and processes of shelf and slope circulation. In: Landry, M.R., Hickey, B.M. (Eds.), Coastal Oceanography of Washington and Oregon. Elsevier Science, Amsterdam, pp. 41–115.

Hickey, B.M., Pietrafesa, L.J., Jay, D.A., Boicourt, W.C., 1998. The Columbia River plume study — subtidal variability in the velocity and salinity fields. J. Geophys. Res. 103, 10339–10368.

Hickey, B.M., Geier, S.L., Kachel, N.B., MacFadyen, A., 2005. A bi-directional river plume: the Columbia in summer. Cont. Shelf Res. 25, 1631–1656.

Horner-Devine, A.R., 2009. The bulge circulation in the Columbia River plume. Cont. Shelf Res 29, 234–251.

Horner-Devine, A.R., Fong, D.A., Monismith, S.G., Maxworthy, T., 2006. Laboratory experiments simulating a coastal river discharge. J. Fluid Mech. 555, 203–232.

Horner-Devine, A.R., Jay, D.A., Orton, P.M., Spahn, E.Y., 2009. A conceptual model of the strongly tidal Columbia plume. J. Mar. Sys 78, 460–475 (this volume).

Jay, D.A., Orton, P.M., Chisholm, T., 2002. Speculations on Human and Climate-Change Alteration of Iron Input to Upwelling Areas off Oregon and Washington, Eastern Pacific Ocean Conference, Timberline Lodge, OR, September 2002.

Landry, M.R., Postel, J.R., Peterson, W.K., Newman, J., 1989. Broad-scale distributional patterns of hydrographic variables on the Washington/Oregon shelf. In: Landry, M., Hickey, B.M. (Eds.), Coastal Oceanography of Washington and Oregon. Elsevier, Amsterdam, pp. 1–40.

Logerwell, E.A., Mantua, N., Lawson, P.W., Francis, R.C., Agostini, V.N., 2003. Tracking environmental processes in the coastal zone for understanding and predicting Oregon coho (*Oncorhynchus kisutch*) marine survival. Fish. Oceanogr. 12, 554–568.

Lohan, M.C., Bruland, K.W., 2006. Importance of Vertical Mixing for Additional Sources of Nitrate and Iron to Surface Waters of the Columbia River Plume: Implications for Biology. Mar. Chem. 98, 260–273.

Macdonald, D.G., Geyer, W.R., 2004. Turbulent energy production and entrainment at a highly stratified estuarine front. J. Geophys. Res. 109, C05004. doi:10.1029/2003JC002094.

Nash, J.D., Moum, J.N., 2005. River plumes as a source of large-amplitude internal waves in the coastal ocean. Nature 43, 400–403.

O'Donnell, J., Marmorino, G.O., Trump, C.L., 1998. Convergence and downwelling at a river plume front. J. Phys. Oceanogr. 28, 1481–1495.

O'Donnell, J., Ackleson, S.G., Levine, E.R., 2008. On the spatial scales of a river plume. J. Geophys. Res. 113, C04017. doi:10.1029/2007JC004440.

O'Reilly, J.E., Maritorena, S., Mitchell, B.G., Siegel, D.A., Carder, K.L., Garver, S.A., Kahru, M., McClain, C., 1998. Ocean color chlorophyll algorithms for SeaWiFS. J. Geophys. Res. 103, 24,937–24,953.

Orton, P.M., Jay, D.A., 2005. Observations at the tidal plume front of a high-volume river outflow. Geophys. Res. Lett. 32, L11605. doi:10.1029/2005GL022372.

Pan, J., Jay, D.A., 2008. Dynamic characteristics and horizontal transports of internal solitons generated at the Columbia River plume front. Cont. Shelf Res 29, 252–262.

Pan, J., Jay, D.A., Orton, P.M., 2007. Analyses of internal solitary waves generated at the Columbia River plume front using SAR imagery. J. Geophys. Res. 112, C07014. doi:10.1029/2006JC003688.

Pearcy, W.G., 1992. Ocean Ecology of North Pacific Salmon, Washington Sea Grant Program. University of Washington Press, Seattle, WA. 179 pp.

Small, L.F., McIntire, C.D., Macdonald, K.B., Lara-Lara, J.R., Frey, B.E., Amspoker, M.C., Winfield, T., 1990. Primary production, plant and detrital biomass, and particle transport in the Columbia River Estuary. Prog. Oceanogr. 25, 175–210.

Souza, A.J., Simpson, J.H., 1997. Controls on stratification in the Rhine ROFI system. J. Mar. Sys. 12, 311–323.

Spahn, E.Y., Horner-Devine, A.R., Nash, J., Jay, D.A., submitted for publication. Particle processes in the Columbia River plume near-field, Submited to J. Geophys. Res.

Thomas, A.C., Weatherbee, R.A., 2005. Satellite-measured temporal variability of the Columbia River plume. Remote Sens. Environ. 100, 167–178.

Van Mol, B., Ruddick, K., 2005. Total Suspended Matter maps from CHRIS imagery of a small inland water body in Oostende, Proceedings of the 3rd ESA CHRIS/Proba Workshop, 21–23 March, ESRIN, Frascati, Italy, (ESA SP-593, June 2005).

Yankovsky, A.E., Chapman, D.C., 1997. A simple theory for the fate of buoyant coastal discharges. J. Phys. Oceanogr. 27, 1386–1401.